Vortex dynamics and the existence of solutions to the Navier–Stokes equations

Alain Pumir and Eric D. Siggia
Laboratory of Atomic and Solid State Physics, Cornell University, Ithaca, New York 14853

(Received 14 July 1986; accepted 2 March 1987)

The Biot–Savart model for a vortex filament predicts a finite time singularity in which the maximum velocity diverges as $(t^* - t)^{-1/2}$ for the time t tending to t^*. The filament pairs with itself, yet remains locally smooth even though the characteristic length scales as $(t^* - t)^{1/2}$. A multiscale perturbative treatment of the Euler equations is developed for solutions that are locally a two-dimensional vortex dipole centered on a slowly varying three-dimensional space curve. For short periods of time the Euler and Biot–Savart solutions agree. Provided this correspondence persists, a sufficiently small viscosity ν will not control the divergence in the maximum velocity until it is of order $\exp(\mathrm{cst}/\nu)$, where cst is a constant of order the filament circulation. Singularities in the Navier–Stokes equations cannot be easily dismissed. The most questionable step in the arguments presented occurs for $\nu = 0$, namely whether the Euler vortex dipole solutions break down when they self-stretch.

I. INTRODUCTION

It is a basic tenet of fluid dynamics that the velocity of an incompressible fluid in a container, if initially a smooth function of space, will remain smooth and bounded for all subsequent times. This assertion is also generally accepted as it applies merely to the existence of solutions even if they are not stable. Under these circumstances, one cannot appeal to a century of careful fluid dynamic experiments as proof that singularities can never occur. The issue then, is whether one can prove from the three-dimensional Navier–Stokes equations that initially smooth solutions remain finite for all times.[1–3] (It has been shown rigorously that finiteness implies smoothness.[1,4])

Mathematicians have not succeeded in establishing this ostensibly simple proposition yet they have put important constraints on how serious a singularity can exist.[1–6] Many very reasonable physical propositions lack mathematical proof; and one would suppose existence problems for Navier–Stokes fall into this class since texts written for physical scientists are utterly silent on these questions. In our view, these questions remain open and debatable even at a physical level of rigor. Dimensional and scaling arguments of the Kolmogorov variety are far from convincing when applied to the exceptional, possibly unstable, and decidedly nonstatistical solutions we find.[7] On the other hand, our solutions may have little physical relevance.

In this article we show by means of a hierarchy of models for vortex tubes together with asymptotic and scaling arguments that solutions to the Navier–Stokes equations can come close to diverging in a finite time. The most problematical step in our argument is the passage from a vortex filament back to a vortex tube obeying the Euler equations. Contrary to cascade theories of turbulence, the remaining step, which restores the viscosity, is simple, more convincing than the usual scaling arguments, and only modifies the inviscid solution when the velocity has already become so large that the incompressibility assumption is untenable. As long as the vorticity remains in tubes the Euler and Navier–Stokes equations have similar singularities. The usual form of dissipation is marginal in that if any power of the Laplacian higher than unity is used there is definitely a viscous cutoff while a lower power renders the dissipation irrelevant. All our arguments suppose a large but finite Reynolds number.

Several caveats should be emphasized. Even though there is always a fixed small expansion parameter that allows one to formally invert the asymptotic analysis that leads from vortex tube solutions of Euler to vortex filaments at any time, there may well be a secular degradation in the correspondence from that time onward. The weakest step in our argument is to demonstrate that tubes remain tubes within the Euler equations. Even if our construction fails at this point, it does so for relatively delicate reasons, thereby invalidating any dogmatic but casual physical arguments that singularities cannot exist. Also for heuristic reasons, developed below, we believe our vortex tube solutions are the most likely candidates for a singularity.

Second, we make no claims about other initial data even though our initial conditions are physically realizable, and the singularities "generic" for vortex tubes. If the scaling that accompanies our solution is believed, then an infinite pointwise velocity implies that the integrated mean square vorticity is also infinite. Cascade ideas predict such a singularity for the Euler equations for all but special initial conditions, but our models shed no light on this important question.[8,9] From internal evidence alone we have no grounds for asserting that our flows have any relevance to turbulence or intermittency. There is, however, a body of laboratory flow visualization experiments and more recently direct numerical simulations that suggest "hairpin vortices" are responsible for the extreme intermittency seen in turbulent boundary layers.[10–14] Hairpins, according to our models, invariably lead to singularities. Our analysis may explain in an idealized way why such large fluctuations are seen in the maximum vorticity and velocity gradients, in the course of a turbulent burst.

 0031-9171/87/061606-21$01.90

Irrespective of any connections with the Navier–Stokes or Euler equations, it is of intrinsic interest to examine how a vortex filament evolves under its own velocity field. This is the simplest continuum dynamical system that admits vortex stretching, which is an essential element in three-dimensional turbulent dynamics. By comparison with two dimensions, there are very few known and interesting time-dependent solutions to the three-dimensional fluid equations, so models are a necessary intermediate step.[15]

In Sec. II we begin with the Biot–Savart model and in successive subsections consider two progressively simpler limits to it. In each case we exploit our earlier observation, documented more fully in this and the following section, that filaments pair antiparallel with themselves and only then proceed to stretch.[16,17] The pairing permits one to replace the Biot–Savart integral by a differential expression in arc length. The stability of a pair of antiparallel straight lines is examined within each model and a number of simple analytic results are obtained.

In Sec. III we present in successive subsections all our numerical results for the Biot–Savart model and its most sensible local version. Salient conclusions are summarized along with pertinent numerical details. Our analytic and numerical results are in sufficiently tight agreement that we consider the Biot–Savart model for a filament pair to be solved.

In Sec. IV we reconsider the asymptotic analysis that reduces a slender vortex tube to a filament in the case when the tube is paired with another of opposite circulation. Incomplete arguments are given for the reverse process, namely how to reconstruct a solution to the Euler equations from filaments that are straight on the scale of their core size. If the Biot–Savart results correctly model the Euler equations, then we argue that viscous effects can be treated in the limit of a quasi-two-dimensional flow subjected to time-dependent stretching.

In the conclusion, we recapitulate the chain of arguments that suggest singularities are not an impossibility for the Navier–Stokes equations. The uncertainties in each step of the argument are stressed. Finally we discuss related numerical work that supports our analysis and mention the experimental evidence for paired vortex tubes in boundary layers.

II. VORTEX FILAMENT MODELS

Once it is decided to replace a vortex tube whose center varies slowly on the scale of its core radius by a space curve plus core parameter, the Biot–Savart formula is the only reasonable dynamical model.[18] We summarize the approximations made in its derivation and justify our ansatz for how the core size responds to changes in the curve. This last argument is ultimately most convincing *a posteriori*. That is, one examines the solutions obtained under the approximation and concludes that the neglected phenomena are indeed irrelevant. It will also be necessary to anticipate the numerical simulations when we derive a local expression for the Biot–Savart integral. Filaments invariably pair so as to achieve zero net circulation. This makes a local approximation considerably more accurate than for the local induction approximation to an isolated filament.

A. Biot–Savart

Imagine an isolated vortex tube with an internal vorticity distribution and core size, σ, uniform along the filament and no axial velocity. Let r_c denote a typical radius of curvature and Γ denote the circulation. Then the velocity at a point either on the axis of the tube[18] or a distance $\geqslant O(r_c)$ away is given by

$$\mathbf{v}(r) = -\frac{\Gamma}{4\pi}\int \frac{[\mathbf{r}-\mathbf{r}(\xi')]\times(d\mathbf{r}/d\xi')d\xi'}{d^{3/2}} + O\left(\frac{\sigma}{r_c}\right)^2, \tag{1a}$$

with $d^2 = [r - r(\xi')]^2 + \alpha\sigma^2$. The details of the core structure enter only α, which is of order unity.[18] We will consistently denote the Lagrangian parameter along the curve by ξ. For a collection of filaments there is, of course, a contribution to the total velocity from each one. To time step the filament we will only need the velocity on the filament itself, say at ξ, and we rewrite the denominator as[19]

$$d = \{[r(\xi) - r(\xi')]^2 + \sigma^2(\xi) + \sigma^2(\xi')\}^{1/2}. \tag{1b}$$

The inessential constant α has been adsorbed into σ. More importantly, we allowed σ to depend on position, and for reasons of symmetry break it into a contribution from ξ and ξ'. Although the quoted errors in (1a) were obtained for σ uniform, we believe they continue to apply when σ varies with arc length, on a scale of r_c. The symmetrical placement of σ is reasonable on physical grounds [one averages $v(r)$ over the tube to obtain $v(r(\xi))$] and guarantees a conserved energy when σ is independent of time, viz.,

$$E = \frac{1}{2}\sum_{ij}\Gamma_i\Gamma_j\int \frac{(d\mathbf{r}_i/d\xi_i)\cdot(d\mathbf{r}_j/d\xi_j)d\xi_i\,d\xi_j}{[(r_i - r_j)^2 + \sigma_i^2 + \sigma_j^2]^{1/2}}.$$

The core size becomes ξ and time dependent since we adjust σ locally to conserve volume:

$$\sigma(\xi)^2\left|\frac{d\mathbf{r}}{d\xi}\right| = \text{cst}. \tag{2}$$

We finally obtain a closed system of equations by insisting

$$\frac{d\mathbf{r}(\xi,t)}{dt} = \mathbf{v}(r(\xi)). \tag{3}$$

It is an entirely unsettled question as to under what circumstances vortex tubes remain tubes as they evolve.[20–22] Even putting aside this question and supposing σ/r_c remains small (which it does for a paired filament), (2) is merely one extreme of a family of models that conserve the volume of the core.

In reality whenever the stretching is nonuniform, axial velocities are established that can transport core area conservatively along the filament.[20–23] In short, σ^2 should satisfy its own evolution equation whose characteristic frequencies will be on the order of $\Gamma/(\sigma r_c)$ to Γ/σ^2. (We justify this range of values when we discuss Ref. 23 in the conclusion.)

If the vortex tubes remain roughly circular, then the core dynamics is *irrelevant* once the paired filament begins to rapidly stretch. In particular (2) does not make the final blow up any more singular than it otherwise would be. Some

support for these assertions comes from recent simulations of Lundgren and Ashurst,[23] who allow for more realistic dynamics in the core than (2) and still find a singularity similar to ours. Their work is reviewed in the conclusion. From our simulations we find (Sec. III A) that σ varies sufficiently slowly with arc length around the approaching singularity and that even if cross-sectional area moves about, there is insufficient time for appreciable rearrangements to occur prior to the singularity.

A second potential problem of (1a) is that the quoted errors do not obviously apply when pieces of filament approach each other on a scale of the core size. Equation (1a) was developed by a multiscale analysis that decomposes the velocity field of a vortex tube into its cross section (with a "fast" scale σ) and the tube center ("slow" scale, r_c). To treat a paired filament, we merely have to consider a cross section that is a vortex dipole. It is then trivial to account for the deformation of one tube by its mate by simply taking a known two-dimensional vortex dipole solution and letting its center vary slowly in three-space. Details are contained in Sec. IV. Suffice it to say that the Biot–Savart formula with rescaled constants is adequate for paired filaments also.

A third deficiency of (1) and (2) is the lack of a conserved energy when σ is time dependent. This is no surprise since axial flows are neglected and the energy in the swirling component of velocity is not accurately represented. We simply are not retaining all the modes contained in the real flow. This is only a problem if the filaments evolve in such a way that when we restore the full vortex tubes, the usual kinetic energy is not conserved. We see no general resolution to this problem and reconsider the energy constraint in the conclusion after seeing the particular form our candidate singularity solutions assume.

It is useful before doing simulations to have some idea of the instabilities a pair of antiparallel vortex tubes is susceptible to. This was first done by Crow who used the Biot–Savart law with a different cutoff than ours.[24] We have repeated his analysis with (1) and (2) for the parameter regime of interest to us, namely with the filament spacing of order the core size.

We consider antiparallel straight filaments of circulation Γ and spacing ρ and define $\beta = (\rho^2 + 2\sigma^2)^{1/2}$. There are two modes, symmetric (S) and antisymmetric (A), which are distinguished by their projection onto the plane defined by the unperturbed filaments or a plane normal to the segment joining them (Fig. 1). Their growth rates α_S, α_A are given by

$$\begin{aligned}
&\alpha_S^2 = (1 - \psi + \zeta)(1 + \chi - \zeta - 4\sigma^2/\beta^2),\\
&\alpha_A^2 = (1 + \psi + \zeta)(1 - \chi - \zeta - 4\sigma^2/\beta^2),\\
&\psi(k) = \tilde{k}K_1(\tilde{k}) + \tilde{k}^2K_0(\tilde{k}),\\
&\chi(k) = \tilde{k}K_1(\tilde{k}),\\
&\zeta(k) = (\rho^2/2\sigma^2)\left[\sqrt{2}k\sigma K_1(\sqrt{2}k\sigma)\right.\\
&\qquad \left. + 2k^2\sigma^2K_0(\sqrt{2}k\sigma) - 1\right],
\end{aligned} \tag{4}$$

where K_0 and K_1 are the usual Bessel functions, $\tilde{k} = \beta k$, and we have suppressed a time scale of $\Gamma/(2\pi\beta^2)$. The growth rates, where positive, are plotted in Fig. 2 for $\sigma/\rho = 1$.

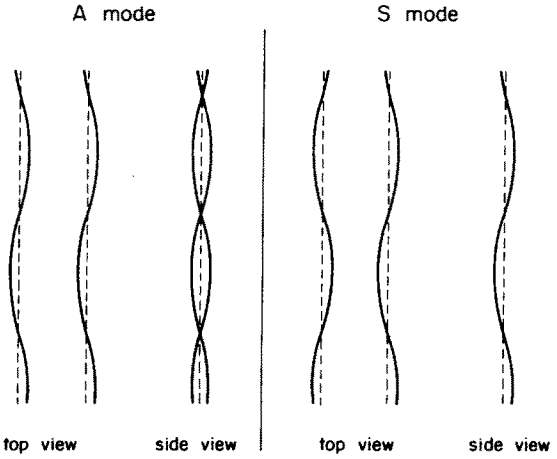

FIG. 1. The antisymmetric (A) and symmetric (S) modes of instability for a pair of antiparallel vortex filaments. The unperturbed filaments are dashed.

For long axial wavelengths and well separated filaments, Crow's (or our) perturbation treatment of Biot–Savart agrees with the results of a complete analysis of the Euler equations for a pair of vortex tubes.[25–27] The most difficult part of a thorough calculation is understanding one tube in the field of the other which may be replaced by a local strain matrix for $\rho \gg \sigma$. For any wavelength, the filament equations can at best only capture the true eigenmodes that have no radial zeros within the core. (Radial is measured outward from the tube axis.) When the axial wavelength is of order σ, an analysis of the Euler equations shows that only the radial modes with zeros are unstable. The precise details depend explicitly on the core structure. Therefore any short wavelength instability predicted by Biot–Savart is spurious and the result of an unjustified extrapolation. There are short wavelength instabilities but one would guess from their eigenmodes that they would disrupt the core rather than merely displacing it bodily.

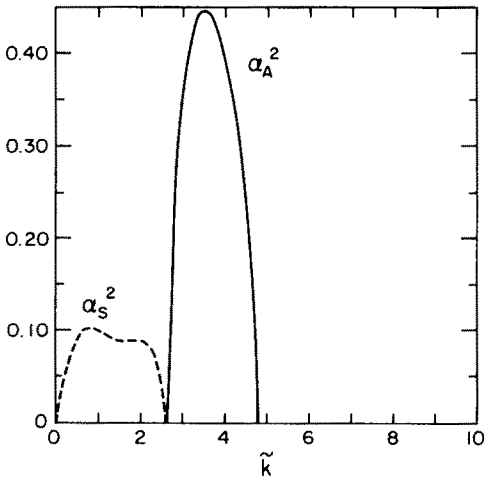

FIG. 2. The growth rates, α_S^2 (dashed) and α_A^2 (solid), for the two modes in Fig. 1 and Eq. (4) as a function of $k\sqrt{\rho^2 + 2\sigma^2}$. The ratio of spacing to core size is $\rho/\sigma = 1$ and frequencies are measured in units of $\Gamma/[2\pi(\rho^2 + 2\sigma^2)]$.

Analysis of the Euler equations becomes much more complicated when the filament spacing is of order σ. The core shape is nontrivial at zeroth order and the influence of one filament on the other cannot be represented as a simple stagnation point flow as before. The complete stability analysis has never been done to the best of our knowledge. We still believe there is a correct long axial wavelength approximation to the Euler equations in terms of filaments (Sec. IV) and that the instability predicted by Biot–Savart is qualitatively and physically correct in this regime.

One should also ask whether the A-mode instability artificially favors the formation of singularities in the filament equations. The answer is decidedly no, since the local limit of Biot–Savart we derive in the next section has no short wave instability yet has quantitatively similar singularities. The reason for examining Biot–Savart at all is that it is clearly the appropriate model in the early stages of the instability. We also wanted to verify that certain qualitative features of the filament dynamics such as the pairing and the inequality $r_c \gg \sigma$ were not limited to the initial stages of the collapse. Lastly, the insensitivity of the singularity to the spectrum of instabilities lends it plausibility at least within a filament approximation.

B. Local model

In order to justify further expansion and reduction of the Biot–Savart integral, we need to anticipate several salient features of the simulations to follow: (a) vortex filaments pair antiparallel with a spacing $\rho \sim \sigma$; (b) the ratio of σ to the local radius of curvature is a small parameter point by point; and (c) the radius of curvature sets the scale of variation with arc length, and the tangent vectors for corresponding points of the paired filaments agree to $O(\sigma/r_c)$.

Equations (1) and (2) become local in arc length when expanded in (σ/r_c). We should further note that when the local equations are time stepped, properties (a)–(c) persist and in fact (σ/r_c) becomes somewhat smaller than it was for Biot–Savart. While we have an analytic argument for (a), we have no proof of (b) or (c) other than simple inspection of the data.

Before entering into the details of the calculation, it is useful to anticipate the form of the answer and state the errors in the expansion. The largest effect, is one filament convecting the other with a velocity $v \sim \Gamma/\max(\rho,\sigma)$. To next order in σ/r_c we have the usual local induction term for each filament, which is of order $\Gamma \ln(r_c/\sigma)/r_c$ and directed along the binormal. We demonstrate by means of an example and more generally in the next subsection that the first effect sets the velocity of the pair while the second brings the two filaments together.

It is well known that the error in the local induction approximation for an isolated filament is $O(1/\ln(r_c/\sigma))$.[28] Let us add to property (c), for the moment, the assumption that corresponding normals on the two filaments agree to $O(\sigma/r_c)$. A local approximation to the Biot–Savart integral is then accurate to $O(\sigma/r_c)$ since the velocity from distant pieces of filament cancels due to the proximity of its mate with opposite circulation.

Numerical simulations of the local model reveal, however, a phenomenon suggestive of a shock in which the normal vectors on one side only of the singularity fail to agree. The configuration one finds is reminiscent of the initial stages of pairing examined in Ref. 16. That is, the two planes defined by the two normals and common tangent form a dihedral. The normals to the planes are the binormals of the curves and point towards the interior of the dihedral. When the binormals are not antiparallel, a certain logarithm of an integral cutoff fails to cancel and the errors in the equations we simulate are no better than for the local induction approximation. However, the component of the binormal, which is not perpendicular to the symmetry plane of the dihedral, acts to retard the interfilament velocity which is a factor (r_c/σ) larger. We will henceforth understand our errors as measured separately for the average and relative velocities of corresponding points on the two filaments since they are intrinsically of different orders (Γ/σ and Γ/r_c). Our only significant error (i.e., order $1/\log(r_c/\sigma)$ vs (σ/r_c), then remains a small reduction in the local induction velocities when the binormals are not antiparallel. We believe this to be immaterial.

Denote the arc length by s and the filament by a subscript 1,2. Then the integrals for the velocity at $r_1(s_1)$ will be broken into a local part $|s - s_1| \leqslant l \sim O(\sqrt{\sigma r_c})$ and a remaining "distant" piece. We say integrals, plural, since whenever two pieces of filament are close one is in the local limit for each irrespective of whether both pieces are eventually connected at some remote point. Local contributions are evaluated with the aid of the series

$$\mathbf{r}(s) = \mathbf{r}(\bar{s}) + (s-\bar{s})\hat{\mathbf{t}}(\bar{s}) + \tfrac{1}{2}[\hat{\mathbf{n}}(\bar{s})/r_c](s-\bar{s})^2 + O(l^3/r_c^2), \tag{5}$$

where $\hat{\mathbf{t}}$ and $\hat{\mathbf{n}}$ denote the unit tangent and normal vectors (at $\bar{s}$) and we assume that the radius of curvature sets the scale of length. We will need the binormal $\hat{\mathbf{b}} = \hat{\mathbf{t}} \times \hat{\mathbf{n}}$ below. The expansion for filament 2 as it enters $\mathbf{v}(r_1(s_1))$ is centered at the point $s_2 = s_2(s_1)$ of closest approach, i.e.,

$$(\mathbf{r}_2(s_2) - \mathbf{r}_1(s_1)) \cdot \hat{\mathbf{t}}_2(s_2) = 0. \tag{6}$$

When arguments are not indicated, we will use subscripts as in $\mathbf{t}_{2,1}$ to denote $\mathbf{t}_2(s_2(s_1))$, where the relevant value of s_1 will be obvious from the context. Let $\boldsymbol{\rho}_{2,1} = \mathbf{r}_1(s_1) - \mathbf{r}_2(s_2(s_1))$. Subscripts in the opposite order will apply to quantities entering the velocity of filament (2) due to filament (1).

The local velocity from filament 1 at $\mathbf{r}_1(s_1)$ is

$$\mathbf{v}_{1,1}(r_1) = \frac{\Gamma_1}{4\pi}\frac{\hat{\mathbf{b}}_1}{2r_{c1}}\int_{-l}^{l}\frac{u^2\,du}{(u^2 + u^4/r_{c1}^2 + 2\sigma_1^2)^{3/2}}. \tag{7}$$

The fractional errors in the numerator are $O(l^2/r_c^2)$ since the symmetry $u \leftrightarrow -u$ eliminates all odd terms in (5). The term u^4/r_c^2 in the denominator may be neglected with a comparable error.

The local contribution from filament 2 to $\mathbf{v}_1$ reads ($\Gamma_2 = -\Gamma_1$)

$$\mathbf{v}_{2,1}(r_1) = \frac{\Gamma_2}{4\pi}\hat{\mathbf{t}}_{2,1} \times \boldsymbol{\rho}_{2,1}\int_{-l}^{l}\frac{du}{d_{2,1}^{3/2}} + \frac{\Gamma_2}{4\pi}\frac{\hat{\mathbf{b}}_{2,1}}{2r_{c2,1}}\int_{-l}^{l}\frac{u^2\,du}{d_{2,1}^{3/2}}, \tag{8}$$

where

$$d_{2,1}^2 = u^2(1 + \boldsymbol{\rho}_{2,1}\cdot\hat{\mathbf{n}}_{2,1}/r_{c2,1}) + \rho_{2,1}^2 + \sigma_1^2 + \sigma_{2,1}^2 + O(l^2/r_c^2).$$

The numerators are correct to the same order as before. The new term in the denominator involving (ρ/r_c) is of order (σ/r_c) and will be dropped. If the s dependence of σ is expanded, the first term vanishes by parity and the remainder is $O(l^2/r_c^2)$.

The integral in the first term of (8) may be extended to infinity with an error of order (σ^2/l^2). The remaining integral in (8) must be grouped with (7) in order for the limit to be taken with an overall $O(\sigma^2/l^2)$ error. It is only at this point where we use $|\hat{\mathbf{b}}_1 - \hat{\mathbf{b}}_2| \sim O(\sigma/r_c)$. The total local velocity becomes

$$\mathbf{v}_1(r_1) = \frac{\Gamma_1}{4\pi}\left[\frac{\hat{\mathbf{b}}_1}{2r_{c1}}\ln\left(\frac{r_{c1}^2}{2\sigma_1^2}\right) - \frac{\hat{\mathbf{b}}_{2,1}}{2r_{c2,1}}\ln\left(\frac{r_{c2,1}^2}{\sigma_1^2+\sigma_{2,1}^2+\rho_{2,1}^2}\right)\right] + \frac{\Gamma_1}{2\pi}\left(\frac{\boldsymbol{\rho}_{2,1}\times\hat{\mathbf{t}}_{2,1}}{\rho_{2,1}^2+\sigma_1^2+\sigma_{2,1}^2}\right). \tag{9}$$

It remains to bound the "distant" or nonlocal part of the integral. Consider a piece of filament beginning at $\bar{\mathbf{r}}$, $|\bar{\mathbf{r}} - \mathbf{r}_1(s_1)| \sim l$, with tangent $\bar{\mathbf{t}}$, extending to infinity in a direction away from $\bar{\mathbf{r}}$ and $\mathbf{r}_1(s_1)$. Its contribution to the velocity at $r_1(s_1)$ is of order

$$\mathbf{v}_{nl} \sim [(\bar{\mathbf{r}} - \mathbf{r}_1)\times\bar{\mathbf{t}}]/l^2.$$

From a pair similarly situated, v_{nl} is no bigger than σ/l^2 and negligible compared to the last term in (9). The contribution to the relative velocity at r_1 and $r_{2,1}$ is $O(\sigma^2/l^3)$ and negligible compared to the remaining terms in (9).

The local model becomes

$$\frac{d\mathbf{r}_i}{dt} = \mathbf{v}_i(r_i), \quad \sigma_i^2\left|\frac{d\mathbf{r}_i}{d\xi_i}\right| = \text{cst}, \tag{10}$$

where $\mathbf{v}_1(r_1)$ appears in (9) and we define $\mathbf{v}_2$ by sending the subscripts $1\to2$ and $2,1\to1,2$. No further approximations are made and, to evaluate $\mathbf{v}_i$, it is necessary to find the closest point on the other filament for every node.

It is instructive to examine the stability of the local model for a pair of straight filaments. This limit is ill posed since r_c is infinite and occurs in a logarithm. We sidestep this difficulty by replacing $\ln(r_c^2/2\sigma^2)$ and $\ln[r_c^2/(2\sigma^2+\rho^2)]$ by two constants $A_1 > A_2 > 0$. This would be reasonable for a pair of circles if we also insisted that $kr_c \gg 1$. The term $\hat{\mathbf{b}}/r_c$ is linearized by rewriting it as $\hat{\mathbf{t}}\times d\hat{\mathbf{t}}/ds$. The arc length is unmodified when one linearizes, so σ is constant. In the same notation and units as in Eq. (4), one finds the dispersion relations:

$$\begin{aligned}\alpha_S^2 &= (A_1 - A_2)k^2[2 - 4\sigma^2/(2\sigma^2+\rho^2) + (A_2 - A_1)k^2],\\ \alpha_A^2 &= -[2 + (A_1 + A_2)k^2][4\sigma^2/(2\sigma^2+\rho^2) + (A_1 - A_2)k^2].\end{aligned} \tag{11}$$

Note that α_S^2 is an inverted parabola in k^2 and qualitatively similar to Fig. 2. The antisymmetric mode is never linearly unstable. Of course our analysis does not rule out algebraic growth in time but there is no sign of it in the simulations of (10) reported in Sec. III B. The change in stability for the A mode in going from (4) to (11) is a useful illustration of precisely what a local approximation picks out. There is no conflict with the stated errors, since r_c was assumed to set the scale on which $\mathbf{r}_i$ varied with arc length. Difficulties occur for perturbations on the scale of σ and the A mode is limited to $k\sigma \sim 1$. Recall from Sec. II A that the Biot–Savart A-mode instability does not carry over to the Euler equations. The local model may be a more sensible version of the Euler equations than (1) and (2) provided instabilities that disrupt the cores can be neglected. The absence of the short wavelength, A-mode instability makes the numerical solutions of the local model look much more regular than those of (1) and (2). That is, the ratio σ/r_c is much smaller, there are not folds on top of folds, and there is only one point singularity rather than many. Nevertheless, that one singularity scales with time in the same way we found with Biot–Savart. Furthermore the reduced value of σ/r_c makes it more plausible (Sec. IV) that a similar solution to the Euler equation can be found. For identical reasons unstable solutions to Biot–Savart should exist that are essentially identical to those of the local model.

It is instructive to illustrate the interplay of the intrafilament, local induction, terms with the interfilament ones by examining a special solution that has no finite time singularity. Consider a vortex ring of radius R that approaches normal to a free slip plane, at a distance $\rho/2$. It will interact with its image behind the plane and expand radially outward. The local model (10), neglecting subscripts that are now superfluous, reads

$$\begin{aligned}\frac{dR}{dt} &= \frac{\Gamma}{2\pi}\frac{\rho}{\rho^2+2\sigma^2},\\ \frac{dp}{dt} &= -\frac{\Gamma}{4\pi R}\ln\left(1+\frac{\rho^2}{2\sigma^2}\right),\\ \sigma^2 R &= \text{cst}.\end{aligned} \tag{12}$$

One sees very clearly that the interfilament velocity is responsible for the vortex stretching since it expands the circles radially. The intrafilament terms contribute only to $d\rho/dt$ and bring the two filaments together. For more general initial conditions these two effects remain. When stretching occurs, the normal vector points inwards and the binormals are directed to bringing the filaments together. A more detailed view of the processes that bring about the pairing was contained in Ref. 16.

In the following subsection, we will derive, more generally than we need for (12), that $\rho^2/\sigma^2 \sim 1/\ln(\sigma^{-1})$ as $\sigma\to0$. Hence, neglecting logs, $R \sim t^2$, $\rho \sim t^{-1}$, so ultimately ρ/σ gets arbitrarily small but only as $(\ln t)^{-1/2}$. Similar slow logarithmic factors that bring the circulation of each filament to zero will appear when we add viscous effects. They are an indication that the usual Laplacian damping formula is marginal. Thus even under the most optimistic assumptions about all other effects, logarithmic corrections will ultimately control any singularity. This is not a real limitation since an immense amount of stretching can occur before $(\ln\sigma)^{1/2}$ becomes appreciable.

This is also an appropriate point to illustrate our earlier remark about how energy conservation has to be imposed on a filament solution. Two paired vortex tubes obeying conditions (a)–(c) above, with no axial velocity, and whose cross-sectional shape is constant will have an energy equal to cst $\Gamma^2 L$, where L is the total length, and "cst" a fixed shape-dependent constant. The density is unity. Note we only insist on a constant shape; σ can vary widely with arc length provided it does so on a scale of r_c. The calculation of $\frac{1}{2}\int_{\text{vol}} v^2$ is trivial having made these assumptions. The velocity as a function of coordinates x,y in the plane normal to the filament axis scales as $(\Gamma/\sigma)\, f(x/\sigma, y/\sigma)$, where f is independent of ξ. The volume integral may be rewritten approximately as $dx\, dy\, ds$. The integral of the kinetic energy over x,y converges for $r_c \gg (x^2+y^2)^{1/2} \gg \sigma$ since we are integrating over a dipole with $\rho \sim \sigma$. The stated result follows with errors of order $O(\sigma/r_c)$ from the variable charge (see Sec. IV A).

Consider the pair of circular vortex tubes in (12) with $\rho \ll R$ evolving under the Euler equations. Since the axisymmetry must persist, there is no axial velocity and the core shape will change when the circles expand. By examining the energy, it is not difficult to guess that the cores should become more ribbonlike with the short side parallel to ρ and the long side along R. Simulations of this flow have recently been done that confirm these remarks.[29] It will be important to monitor the total arc length when we approach the singularity predicted by the filament models. If nonuniform stretching induces an axial flow the energy constraint becomes that much more stringent.

C. Analytic properties of a simplified local model

While (10) no longer involves an integral over the filament, it is hardly analytically tractable. This is due to the intricate way in which the Frenet–Seret data for the two filaments enter as well as quantities such as $\rho_{1,2} \neq \rho_{2,1}$. The obvious simplification we will pursue here is to resort to average and relative variables for corresponding points on the two filaments. There is then a single $\boldsymbol{\rho}$ and a single $\mathbf{r}$ from which the tangent, normal, and curvature are derived. There is general agreement with the paired ring example in Sec. II B as regards the general effects of inter- and intrafilament velocities. The important difference is that we now have information that is truly local in ξ obtained without the assumption of axisymmetry that led to (12). The time dependence is completely different and singularities will emerge in a finite time.

Further reduction of (10) requires the assumption that $\hat{n}_1$ and $\hat{n}_2$ are parallel. To the extent this is untrue, the local induction velocity should be reduced by a numerical factor as was discussed in Sec. II B. Everything that follows in this section would be unaffected. The parallelism of the two tangents is obvious from the pictures. Since the approximations required to simplify (10) are of the same accuracy as involved in deriving the model itself, why should one bother with (10) at all?

The problem is that these small changes drastically modify the stability properties at high k. The A mode [cf. Eq. (11)] remains stable but the second k-dependent term in the S mode that stabilized it at large $|k|$ disappears, so that the unstable frequency goes as $\alpha_s \sim \text{cst}|k|$ for all $|k|$. The positive constant depends only on (σ/ρ).

Of course we do not believe any of these models for $k\sigma \sim 1$. One can also explicitly see for high k why the Crow eigenmodes for a line violate the condition $|\hat{b}_1 \cdot \hat{b}_2| = 1 - O(\sigma/r_c)^2$. It is not surprising that the eigenfrequencies for $k\sigma \sim 1$ change. If one attempted to simulate this simplified local model, the high k singularities would be much in evidence and destroy the computation. Since the local model of Sec. II B does give rise to smooth solutions, any analytic results we derive from its simplified version here should apply to $O(\sigma/r_c)$.

With these warnings, let us write an equation for $\mathbf{r} = \frac{1}{2}(\mathbf{r}_1 + \mathbf{r}_2)$ by averaging the $\mathbf{v}_1$ and $\mathbf{v}_2$ equations from (10) and replacing $\hat{\mathbf{t}}_i$ and $\hat{\mathbf{n}}_i/r_{ci}$ by $\hat{\mathbf{t}} = d\mathbf{r}/ds$ and $d^2\mathbf{r}/ds^2$, respectively. Only a single $\boldsymbol{\rho}$ variable is used as well as a single σ. We chose length factors such that $\sigma^2\, ds/d\xi = 1$ and adsorb $\Gamma/4\pi$ into the time scale. Then

$$\frac{d\mathbf{r}}{dt} = \frac{1}{\rho^2 + 2\sigma^2}\, \boldsymbol{\rho} \times \partial_s \mathbf{r}, \tag{13a}$$

$$\frac{d\boldsymbol{\rho}}{dt} = \frac{\hat{\mathbf{b}}}{2r_c} \ln\left(1 + \frac{\rho^2}{2\sigma^2}\right) - \frac{\boldsymbol{\rho} \times \partial_s \boldsymbol{\rho}}{\rho^2 + 2\sigma^2}, \tag{13b}$$

$$\sigma^2\, \partial_\xi s = 1, \tag{13c}$$

where ∂_ξ and ∂_s denote partial derivatives and $\hat{\mathbf{b}} = \hat{\mathbf{t}} \times \hat{\mathbf{n}}$. In order to consistently identify $\boldsymbol{\rho}$ as the (normal) distance between the filaments, we require that if $\boldsymbol{\rho} \cdot \partial_\xi \mathbf{r} = 0$ initially, it remains so for all time [recall (6)]. Therefore we compute

$$\frac{d(\partial_\xi \mathbf{r} \cdot \boldsymbol{\rho})}{dt} = \boldsymbol{\rho} \cdot \partial_\xi \left(\frac{1}{\rho^2 + 2\sigma^2}\, \boldsymbol{\rho} \times \partial_s \mathbf{r}\right) - \frac{\partial_\xi \mathbf{r} \cdot (\boldsymbol{\rho} \times \partial_s \boldsymbol{\rho})}{\rho^2 + 2\sigma^2} = 0. \tag{14}$$

In the first term on the right, the ξ derivative must act on $\boldsymbol{\rho}$ since otherwise it is zero. Derivatives with respect to s or ξ are proportional so the entire right-hand side is zero.

Of more interest is an equation for the cumulative stretching $\partial_\xi s$. From (13a),

$$\partial_\xi s \frac{d}{dt}(\partial_\xi s) = \partial_\xi \mathbf{r} \cdot \partial_\xi \left(\frac{\boldsymbol{\rho} \times \partial_s \mathbf{r}}{\rho^2 + 2\sigma^2}\right) = \frac{[\partial_\xi(\partial_s \mathbf{r}) \times \partial_\xi \mathbf{r}] \cdot \boldsymbol{\rho}}{\rho^2 + 2r^2} = \frac{(\partial_\xi s)^2 (\boldsymbol{\rho} \cdot \hat{\mathbf{b}})}{(\rho^2 + 2\sigma^2) r_c}. \tag{15}$$

Furthermore

$$\frac{1}{2}\frac{d\rho^2}{dt} = \boldsymbol{\rho} \cdot \hat{\mathbf{b}}\, r_c^{-1} \ln\left(1 + \frac{\rho^2}{2\sigma^2}\right). \tag{16}$$

By taking the ratio of (16) to (15) and using $\sigma^2\, \partial_\xi s = 1$ we can derive an equation for $y = \rho^2/2\sigma^2$ as a function of $x = \ln(\sigma^{-1})$,

$$\frac{dy}{dx} = -2(1+y)\ln(1+y) + 2y = -y^2 + O(y^3). \tag{17a}$$

It is remarkable that a closed equation for $\rho(\sigma)$ exists. It can readily be cast in the form of a Lyapunov functional which predicts that any $y > 0$ will relax to $y = 0$ (i.e, the

right-hand side is negative and monotone decreasing for all $y>0$). This is the most compelling analytic argument we can give for the pairing. In the numerical simulations, a slow decrease in ρ/σ consistent with

$$y = 1/(\text{cst} + x) \tag{17b}$$

is in fact seen. (Here cst is an arbitrary constant.) Note that the "binding" implied by $y\to 0$ only operates when $\sigma\to 0$ or $\partial_\xi s\to\infty$, i.e., in response to stretching and irrespective of the actual time. The Lyapunov form of (17a) suggests that the two filaments remain tied together even when various $O(\sigma/r_c)$ terms are restored. There is no guarantee then that $y\to 0$ but merely that it remains $O(1)$ or less.

Several more interesting properties of the collapsing solutions follow if we input two qualitative results from the numerical simulations;

$$\sigma/r_c \sim \text{cst}, \tag{18a}$$

$$-\boldsymbol{\rho}\cdot\hat{\mathbf{b}}/|\rho| > \text{cst} > 0. \tag{18b}$$

The two free constants are of course independent and for σ/r_c we really only need to assume that it lies between two constants. Let us further neglect logarithms and set $\rho/\sigma = 1$.

Then we find

$$\frac{d}{dt}(\partial_\xi s) = \text{cst}\, s_\xi^2, \quad \sigma^2 \sim (t^* - t). \tag{19}$$

In the last line, t^* is by definition the singularity time for the point ξ and an overall constant of order (σ/r_c) has been neglected. In Sec. IV we work systematically in the small parameter σ/r_c and show $\sigma^2/(t^*-t)$ is indeed of this order. For the moment note that σ^2 is constant for two straight lines, i.e., $r_c = \infty$.

It will be of some importance to estimate how the total length L grows due to a single point singularity. Our interest in this quantity stems from the implicit constraint energy conservation imposes on the dynamics of a filament if it really corresponds to a vortex tube. Recall our earlier argument that the total energy of a vortex pair scales as the length, if the shape is constant and the axial velocity negligible.

Think of the filament pair as a triangle with the singularity at its apex. Close to t^*, the legs are effectively frozen while the apex moves a distance $\sim\int_t^{t^*}(\Gamma/\sigma)dt \sim \text{cst}\cdot\sigma(t)$. Therefore the total length is

$$L = L^* - \text{cst}\,\sigma(t). \tag{20}$$

We will verify this behavior numerically in Sec. II B.

At a purely formal level it may be shown from property (18b) above that L diverges in a finite time if $\max|r|$ is uniformly bounded in time. We say "formal" since as we have just shown point singularities develop first. Any connection between a filament model and the Euler equations is dubious after that point. Purely within the context of this model, since the curvature appears in the equations themselves and becomes infinite at one point with L finite; the manipulations we have to perform in order to show L subsequently diverges may be meaningless. The restriction on $|r|$ is a technical necessity to rule out the ring pair example in Sec. II A for which $L\sim t^2$. The long wavelength S mode furnishes enough instability that any derivation from circular symmetry will lead to local folding, stretching, and pointlike singularities in a finite time. The argument for infinite L proceeds as follows.

Assume we have a closed curve parametrized by $\xi\in[0,1]$ with length L. Then,

$$L = \int ds = -\int(\partial_s\hat{\mathbf{t}})\cdot\mathbf{r}\, ds < \max|r|\int r_c^{-1}\, ds. \tag{21}$$

Equation (15) implies, with our earlier assumptions ($\text{cst}>0$ is a free constant in each equation),

$$\frac{d(\partial_\xi s)^{1/2}}{dt} = \frac{\text{cst}\,\partial_\xi s}{r_c}.$$

Then

$$L^{1/2} \geqslant \int(\partial_\xi s)^{1/2}\, d\xi = \text{cst}\int_0^t dt\left(\int r_c^{-1}\, ds\right) > \text{cst}\int_0^t L(t).$$

These inequalities imply that $\int_0^t L(t)$ blows up in a finite time, and hence L itself does. This collection of simple analytic solutions has hopefully given the reader some intuition for the numerical results to follow.

III. NUMERICAL SIMULATIONS

A. Biot–Savart

In this section we integrate the full Biot–Savart equations for a single closed filament with the core size adjusted locally, (2). The initial data was the same as in Ref. 16 where σ was independent of ξ and adjusted to maintain the total core volume constant. Without pictures of r for a sequence of times and certain other diagnostics it would be difficult to distinguish the two sets of data. The pairing and stretching look quite similar.

The first singularity obtained with (2) is close to pointlike, so to maintain adequate resolution, we periodically cut off pieces of filament well removed from the incipient singularity. Occasionally two distant points looked equally singular in which case only one was chosen. The errors attributable to this procedure are negligible in view of the pairing and the rapid collapse. These and other numerical details are contained in Sec. III C. Clipping the ends of the filament permits us to observe a 100 times greater decrease in σ^2 than was feasible in Ref. 16. The reader should keep in mind when viewing our output that the maximum velocity and vorticity scale as $\Gamma/\sigma_{\min}$ and $\Gamma/\sigma_{\min}^2$, respectively, where $\sigma_{\min}$ is the minimum value of σ.

Figure 3 shows the initial data after significant pairing has occurred and just after the closed loops on the ends were cut off. Just prior to the cut, the total arc length was 21 compared to its initial value of 11, and $\sigma_{\min} = 0.076$, compared to $\sigma(t=0) = 0.2$. The stated times give one a qualitative impression of how rapidly the collapse ensues after pairing. The time scale is set by $\Gamma = 4\pi$.

Figure 4 is a continuation of the previous figure to a time just before it is necessary to make a second cut. The total arc length has increased by a factor of 2, $\sigma_{\min}$ decreased by the same factor, and the minimum radius of curvature by 4. The latter quantity is the best measure of the folding, which is clearly visible and is driven by the instabilities mentioned at the end of Sec. II A. The lower-middle portion of Fig. 4 is then cut out and evolved until the time shown in Fig. 5. While $\sigma_{\min}$ has decreased by 2 and r_c by somewhat more

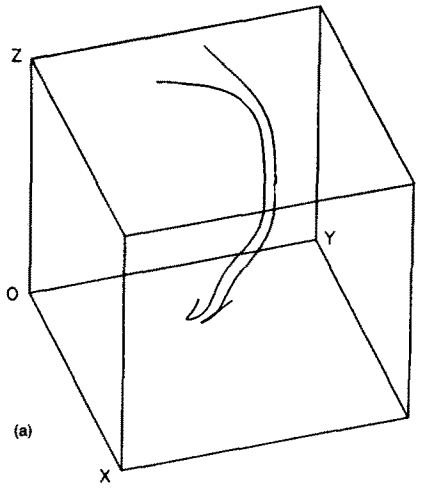

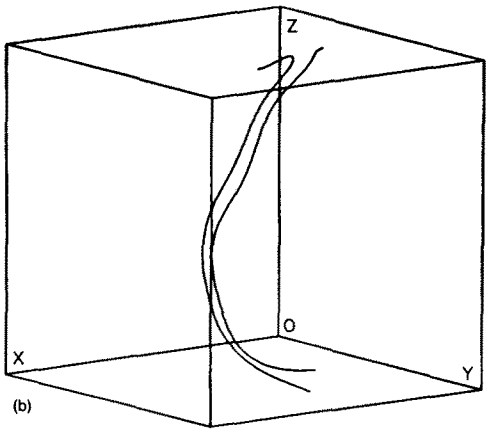

FIG. 3. (a) and (b). Two views of filament pair produced by evolving the twisted ellipse in Ref. 16 forward in time according to Eqs. (1) and (2). The time is 0.976, $\sigma_{\min} = 0.076$, $r_{c\ \min} = 0.59$, and the box size = 3.5.

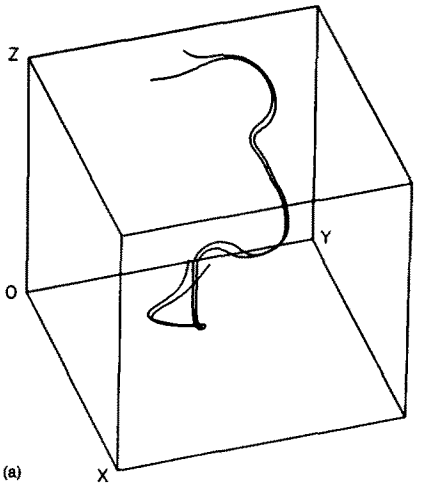

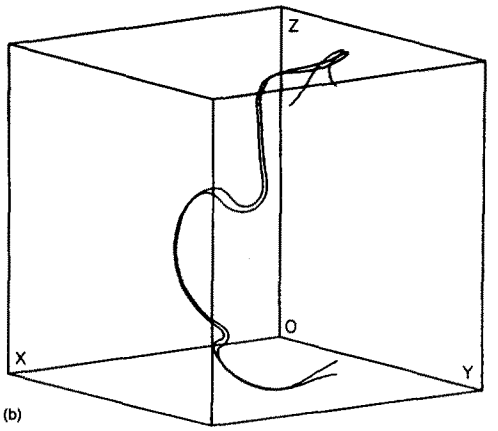

FIG. 4. (a) and (b). Continuation of Figs. 3(a) and 3(b) to $t = 1.1127$. The box size is 5.0, $\sigma_{\min} = 0.038$, and $r_{c\ \min} = 0.16$.

from Fig. 5, the ratio r_c/σ in the region of greatest stretching is still about 8.

In Fig. 6 we have cut out the lower quarter of Fig. 5. On this expanded scale the filaments look smooth and analytic. The integration was continued until $\sigma_{\min}$ decreased by a further factor of 4.5 and $t = 1.161\,995$. It was necessary to make two further cuts to achieve this degree of stretching. The pictures, except for magnification, would look quite similar to what we have already shown. Note there is no tendency for the filament pair to pair further in order to stretch. We observed repeated pairing only at one late time in one out of several runs and consider it to be coincidental and unrelated to the singularity.

The next group of figures shows the core size, filament spacing, and radius of curvature as a function of arc length for a common time $t = 1.158\,04$. Note (Fig. 7) that the core size is within 30% of its minimum value over an arc length of order $100\,\sigma_{\min}$. This, together with the rapid development of the instability, justifies our neglect of dynamical processes that distribute the core area along the filament. We will be more quantitative in the conclusion where we examine an actual model from Ref. 23 of how the axial velocity builds up in response to a nonuniform $\sigma^2(\xi)$. For later use, the one other dimensionless number we need is $\Gamma(t^* - t_0)/[4\pi\sigma^2_{\min}(t_0)] \sim 20$–$50$. (This ratio is independent of the time origin t_0 provided it falls in the scaling regime.)

The filament spacing ρ is plotted on the same scale as σ to facilitate comparison. It will be seen in Fig. 7 that $\rho/\sigma \sim 1$ point by point. The ratio decreases slowly with time as suggested by (17b).

The radius of curvature plots [Figs. 8(a) and 8(b)] are a convincing demonstration that the filaments are smooth and there are no unexpected numerical instabilities. What appears to be numerical noise around an arc length $s \sim 1.3$ when expanded in Fig. 8(b) reveals a series of cusps with a spacing $\sim 8\sigma_{\min}$. At other times, presumably closer to the initiation of the instability, the cusps are spaced by ~ 4–$5\sigma_{\min}$.

This is a signature of the Crow instability though for the

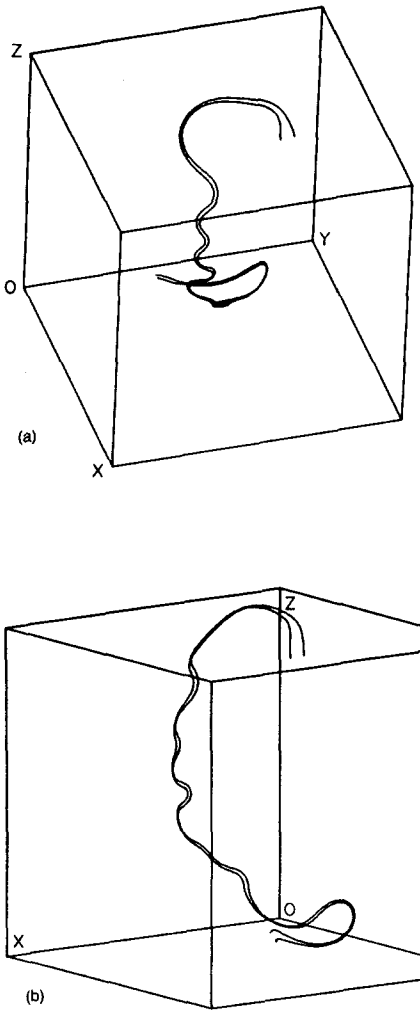

FIG. 5. (a) and (b). Further evolution of the lower middle region of Figs. 4(a) and 4(b) to $T = 1.1475$, where $\sigma_{\min} = 0.021$, $r_{c\,\min} = 0.060$, and the box size = 3.1.

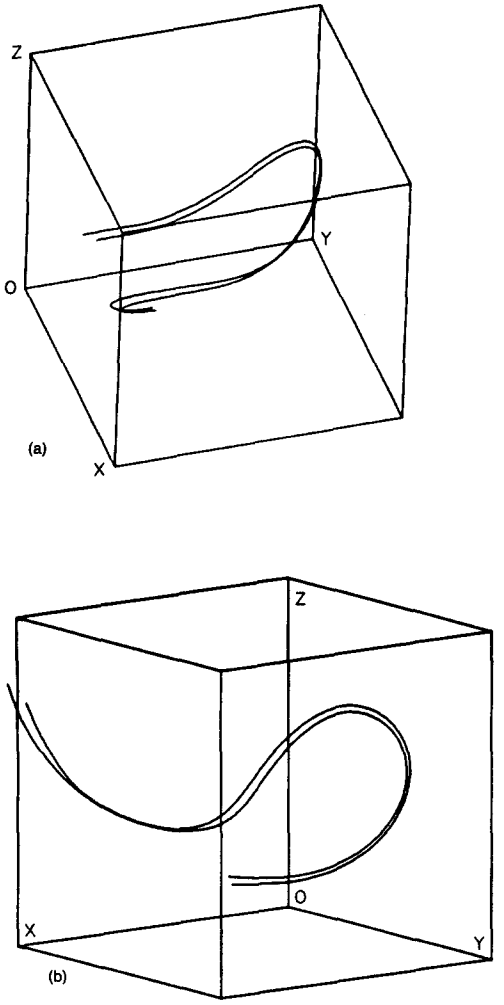

FIG. 6. (a) and (b). Detail of Figs. 5(a) and 5(b) a short time later, $t = 1.1490$. There are approximately 200 computational nodes on each section of filament with an average spacing of one-half the local value of σ. The filaments look no less smooth out to the final time reached by the integration, $t = 1.1620$.

reasons advanced below it is difficult to tell whether the A or S mode is really responsible.[24] The value of r_c/σ is maintained considerably larger than unity by a sort of dynamic equilibrium while the filament itself is approaching a singularity with both r_c and σ tending to zero. When r_c/σ is small (i.e., ~ 4) the stretching rate is greatest, i.e., for a circle $r_c^{-1}\, dr_c/dt \sim (\Gamma/\sigma^2)(\sigma/r_c)$. The stretching both increases r_c and decreases σ because of the constraint on core volume. It also increases the wavelength of an instability as it grows rendering it less unstable. What begins as an A mode may evolve into the region where only the S mode is unstable. For r_c/σ too large, the instabilities initiate new folding and a small r_c. The rather regular cusps in Fig. 8(b) are evidence that a considerable piece of filament is going unstable at once. The ripples in the $\sigma(s)$ curve (Fig. 7) are a vestige of successive episodes of stretching and folding.

The ratio r_c/σ can be assessed by comparing Figs. 7 and 8. Looking over all our data we find this ratio to be at least 4–5 except for $\sim 25\%$ of the times and then only 5% of the points when it fell to 2–3. Although a large value of this ratio

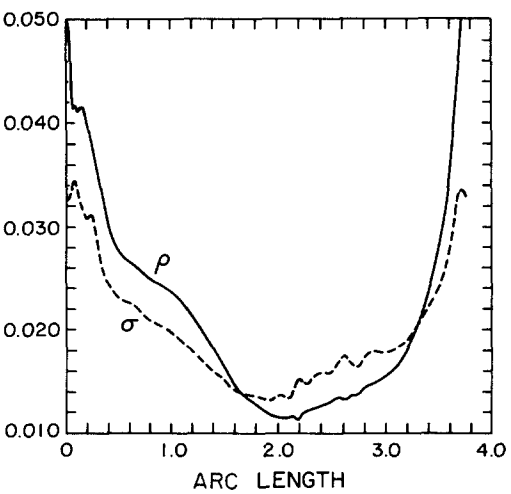

FIG. 7. The filament spacing ρ (solid) and the core size σ (dashed) as a function of arc length at $t = 1.1580$, near the end of the run. The small ripples in σ are the result of the Crow instability causing renewed folding and stretching on small scales as explained in the text.

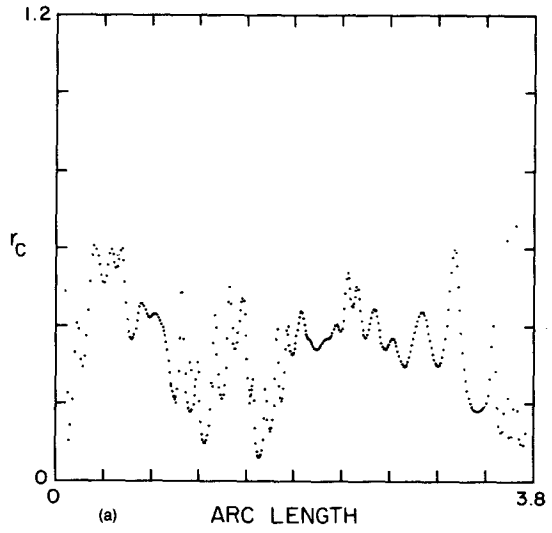

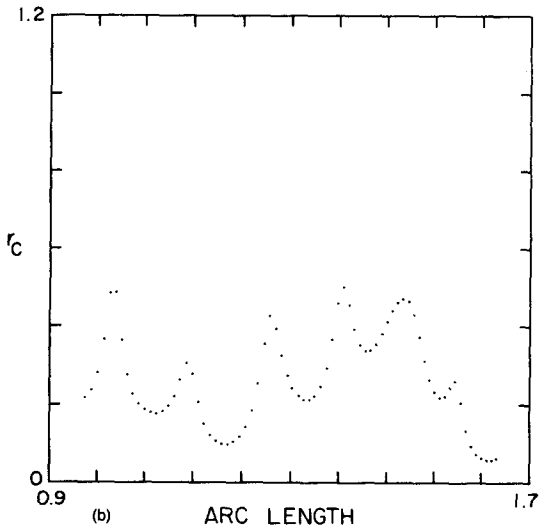

FIG. 8. (a) and (b). The radius of curvature as a function of arc length s for the same data as in Fig. 7. A point is plotted for each computational node. The enlargement for $s = 0.9$–1.7 shows that what appeared to be a numerical instability in the previous graph is actually well resolved. The regularly spaced cusps are a signature of the Crow instability. The ratio r_c/σ is never less than 3.5.

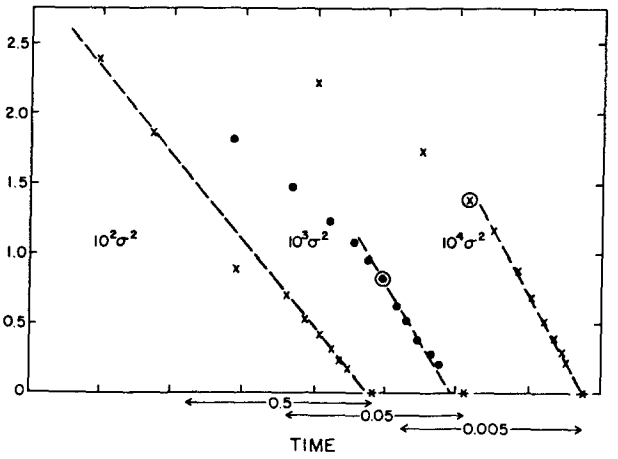

FIG. 9. The minimum of σ^2 as a function of time for the data in Figs. 3–8. A common value of t^* is marked with a star on the abscissa and successive enlargements are offset for clarity. The first two points in each series repeat the previous one. At the circled points, the location of the minimum has jumped to another point on the filament.

is necessary for the approximations through which Biot–Savart is derived from Euler; there was no guarantee that the filament would not develop cusps with $\sigma > 0$. The fact that it does not is a significant result and clearly necessary for there to be any hope of recovering at later times solutions to the Euler equations from those of Biot–Savart.

Data for $\sigma^2_{\min}$ as a function of time are shown in Fig. 9. Linear scales are used and the data points closer to t^* are scaled up and shifted to make them more visible. The values of σ^2 for corresponding points on the paired filaments are always nearly equal and scale together. There is no doubt that $\sigma_{\min}$ hits zero at a finite t^* and varies roughly linearly in time with corrections that could be fit with logarithms in $(t^* - t)$. The small breaks in slope in Fig. 9 occur when the location of the minima jumps to another node on the filament. Since we know well separated points on the paired filaments are dynamically independent there will be many points that collapse. The set of singularities must clearly be thought of as a subset of space-time.

Since we periodically truncate our filaments, it is difficult to say by how much the total arc length grows by t^*. The simultaneous presence of many incipiently singular regions causes the Biot–Savart model to produce much more new filament than its local version where there is only one singularity evident.

B. Local model

The local approximation to Biot–Savart derived in Sec. II B does not have the short wavelength A-mode instability and consequently except for a single pointlike singularity, the entire curve looks very regular. It was not necessary to continuously cut off the filaments away from the singularity in order to maintain adequate numerical accuracy with a manageable number of nodes. In fact the total length increased by a factor of 4 while $\sigma^2_{\min}$ decreased by 500. One awkward feature of (10) as regards its numerical implementation is the need to identify, for each mode, the nearest point on the opposite filament. Details of resolution and step size are relegated to Sec. III C.

It is necessary, in order to apply the local model, that the two filaments start off reasonably close. Accordingly we began with two twisted ellipses with $\sigma = 0.05$, a mean spacing $\rho = 0.15$, and a total arc length $L = 4.0$. Of course the net circulation of the pair was 0 and $\Gamma = 4\pi$. Simply restarting the Biot–Savart results at intermediate times using (10) gave what might be considered more "physical" initial conditions. There was no change in the subsequent evolution from what we find below.

The entire ellipse at the final time is shown in Fig. 10.

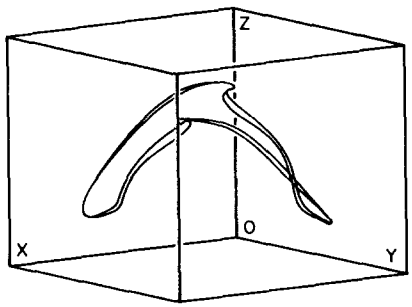

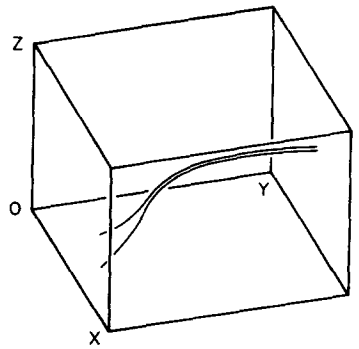

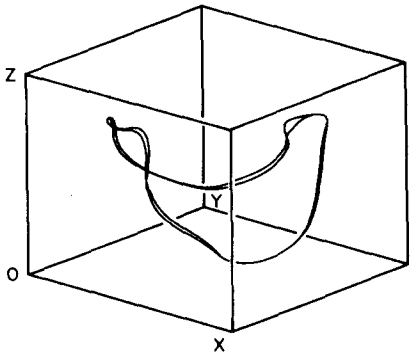

FIG. 10. A pair of ellipses evolved under the local model (10).

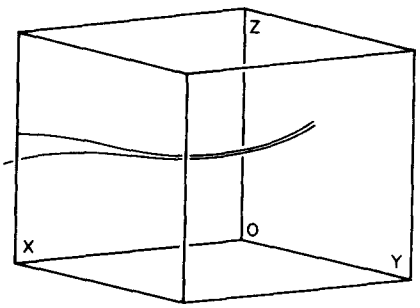

FIG. 11. Blowup of the region around the singularity in Fig. 10.

The location of $\sigma_{\min}$ is determined early in the evolution and does not vary. An enlargement of the region around the singularity is shown in Fig. 11. The asymmetry is real and not an artifact of perspective. It is not understood analytically. The largest errors in $|\hat{\mathbf{n}}_1 - \hat{\mathbf{n}}_2|$ occur just to the left of the singularity.

Figure 12 shows the core size and separation as a function of arc length at the final time. At earlier times the shape is very similar except that the minimum is less pronounced. Points to the right of the singularity where σ rises most steeply correspond to the left side of Fig. 11 where the filaments are separated.

Another important property of these solutions is the value of σ/r_c (Fig. 13). Near $\sigma_{\min}$, $\sigma/r_c \sim 0.05$. There are a few points some 25 nodes away from $\sigma_{\min}$, where $\sigma = 7\sigma_{\min}$ and σ/r_c gets as large as 0.2. Otherwise, the value of σ/r_c at $\sigma_{\min}$ is indicative of the ratio elsewhere on the curves. The local model provides the filament solution most likely to persist when we attempt to generalize to the Euler equations (Sec. IV). Figure 14 plots $\sigma^2_{\min}$ versus time in a manner analogous to Fig. 9. In spite of the very different gross morphologies of the two solutions, the time dependence of $\sigma^2_{\min}$ is very similar. (Note that the slight positive curvature visible in Fig. 14 is also discernible in Fig. 9 if one restricts attention to σ^2 at a fixed Lagrangian point.) This is confirmation that the dynamics is indeed local and unaffected by the additional instabilities present for Biot–Savart. The data are also in accord with Sec. II C where we show that $\sigma^2_{\min}/(t^* - t)$ is constant to within logs.

Figure 15 shows how the total arc length varies in time. The cusp predicted in Eq. (20) is clearly evident.

C. Numerical methods and errors

Our code for integrating (1) and (2) is identical to the one employed in Ref. 16, and we do not intend to reiterate the extensive diagnostics we presented there. The curve was fit with cubic splines which connected the nodes whose position was tracked in time. The spline interpolation facilitated

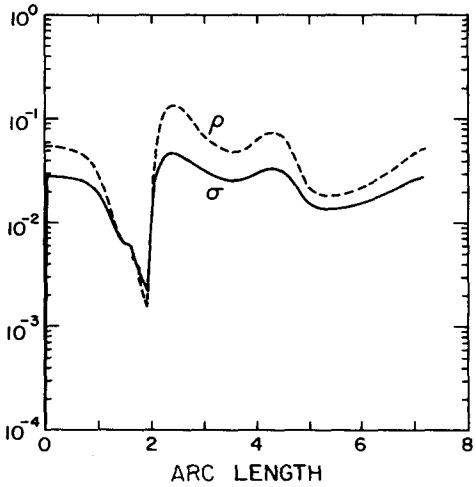

FIG. 12. The core size (solid) and filament spacing (dashed) as a function of arc length at the final time $t = 0.058\,31$. Their initial values at $t = 0$ were 0.05 and 0.15, respectively.

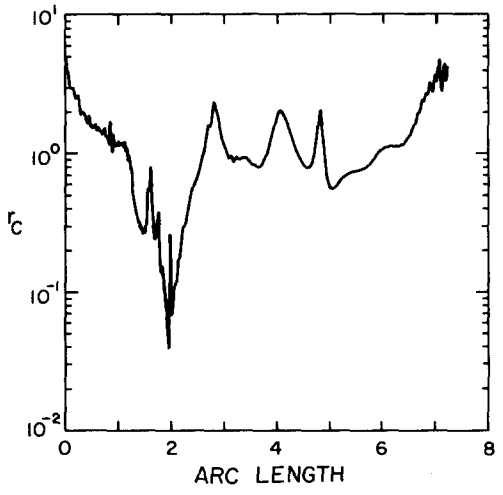

FIG. 13. Radius of curvature as a function of arc length for the same data displayed in Fig. 12. Some of the high frequency structure for $s \lesssim 1$ and $s \sim 7$ may be numerical. In the vicinity of $s = 2$, $r_c/\sigma \sim 20$.

the computation of derivatives. The integrand in (1) was done by Simpson's method with one or more points interpolated between the nodes. The local induction piece was subtracted off from the integrand before the numerical integral was done and then evaluated analytically and added back. Time advancement was done by a fourth–fifth-order Runge–Kutta Fehlberg[16] algorithm with automatic step size adjustment. When stiffness becomes a problem, which it does for the local model, an explicit method is inefficient but the step size was adjusted downward to maintain accuracy. It is essential that (2) be imposed as a constraint. That is, whenever the denominator (1b) is evaluated then the current value of r must be used to find $\sigma(\xi)$.

The curvature, stretching, and nodal spacing were computed at every node and every time step. We therefore claim to have *a priori* error bounds on all integration and interpolation errors. The nodes were periodically redistributed and new nodes added to maintain accuracy. The errors induced by the remeshing were of order 2×10^{-6} in r (when the total length was ~ 2) and 10^{-3} in the tangent vector. The relative errors in the curvature or d^2r/ds^2 were one percent. In the region of greatest curvature, where one would expect the largest errors in computing the velocity, the node spacing was held to one-half the local σ. From the data in the Appendix of Ref. 16 we estimate the relative errors in the intrafilament velocity to be 10^{-5} and several times larger in the interfilament velocity.

We have never seen any evidence of oscillations on a scale smaller than r_c which is generally at least ten times the node spacing. In Ref. 30 the internode spacing was bounded below by 2σ in an effort to suppress the spurious A-mode instabilities (cf. Sec. II A). Since they seem not to have subtracted out the local induction piece and treated it analytically, one would surmise that the integral over nearby pieces of the filament was not done terribly accurately. Nevertheless we have no reason to believe that their results are significantly in error. We have never seen numerical instabilities which are not simultaneously real instabilities of Biot–Savart (Ref. 16, Appendix).

For the local model, σ/r_c was always much smaller than for Biot–Savart so our minimum nodal spacing was kept to the local value of σ. The interpolation and time advancement were the same as employed for Biot–Savart. The remeshing errors were at worst a factor of 2 larger than for the Biot–Savart runs. These quantities are probably the best guide to the accuracy of v in (10) since the expression involves only derivatives of r.

IV. PERTURBATIVE TREATMENT OF THE CONTINUUM EQUATION

In this section we set up the asymptotic analysis that reduces nearly straight vortex pair solutions of the Euler

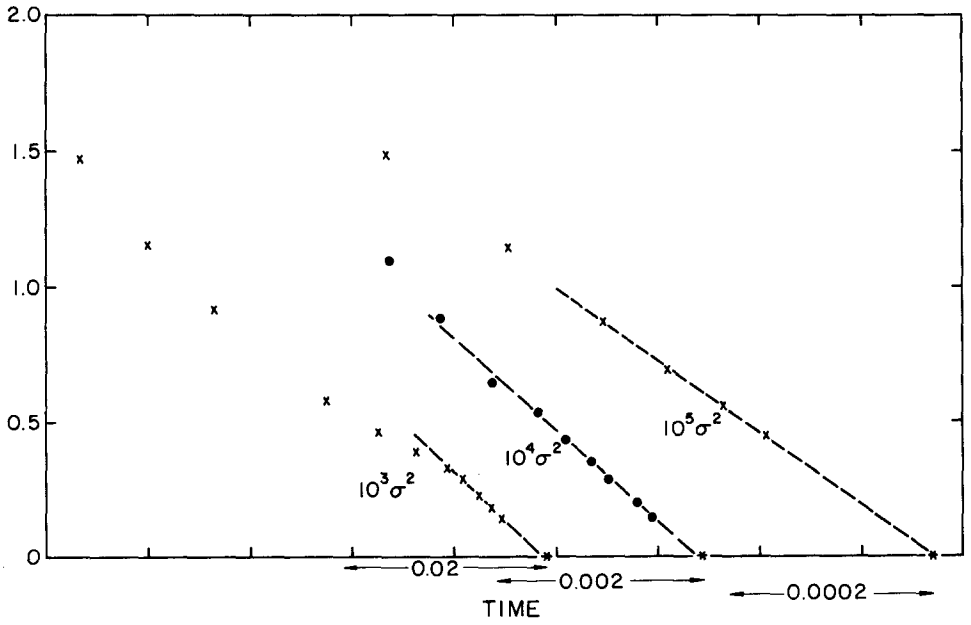

FIG. 14. The minimum of σ^2 as a function of time for the local model plotted in a manner analogous to Fig. 9.

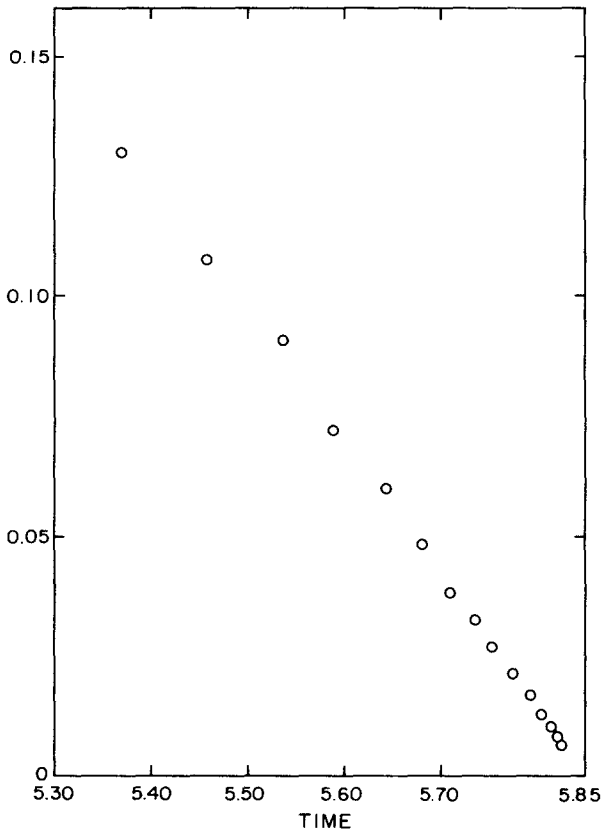

FIG. 15. A plot of $(dL/dt)^{-2}$ versus time showing that the arc length L has a $\sqrt{t^*-t}$ cusp near the singularity for the local model.

equations to local equations for the center of the pair and core size. We also obtain an indication of the internal axial flows that are set up when the vortices stretch nonuniformly. Our expansion does not go far enough to answer the most significant question as to how much distortion takes place in the Euler solutions when the filament equations predict a singularity. Thus while at any point in time a vortex pair solution with the vorticity confined to an approximately circular region should initially obey our model equations, the correspondence may degrade in time rendering the models inapplicable. It is known in other vortex problems that an envelope description can go completely wrong in a finite time due to the formation of discontinuities which invalidate the assumed separation of scales.[21] Preliminary numerical results point in this direction.[31] (The same caveat of course applies to the derivation of the Biot–Savart model (1) from the Euler equations.) Granting that shape distortions are bounded, in Sec. IV B we show that viscous effects are not likely to modify the Euler solutions.

A. Euler equations

Previous derivations of the Biot–Savart equations do not apply to paired vortex tubes since the cores of each are strongly deformed by the other. Of course this is largely a technicality since our simulations still allow us to assume σ/r_c is a small parameter. The fluid mechanics problem is then in zeroth order, just two dimensional with the third dimension entering in next order. Much of the necessary formalism can be borrowed from the earlier analysis of Biot–Savart with the important modifications that the "core" is now a vortex dipole.[18,25]

It is well known from two-dimensional simulations that there are many stable vortex dipole solutions to the Euler equations.[15] In Ref. 32, merger was observed between like signed vortex blobs even while one of them was bound in a dipole. The dipole was not disrupted and there was no intermingling of oppositely signed regions of vorticity. Of course the new entity moved along a different trajectory but a bound configuration of plus and minus vorticity appears very robust. A convenient form for analytic work is the dipole solution obtained by solving $\omega = \nabla^2\psi = -\kappa^2\psi$ for the streamfunction ψ.[33] If β_1 is the first zero of the Bessel function J_1, then $\kappa = \beta_1/a$ and

$$\psi = u\left(r - \frac{2J_1(\kappa r)}{\kappa J_0(\kappa a)}\right)\cos\theta, \quad r<a,$$
$$= ua^2\cos\theta/r, \quad r\geqslant a. \tag{22}$$

The vorticity is confined to $r\leqslant a$ and the circulation of either semicircle of the dipole is

$$\Gamma = \frac{4\kappa^{-1}u}{J_0(\kappa a)}\int_0^{\beta_1} J_1(x)x\,dx.$$

In terms of a right-handed coordinate system $\hat{\mathbf{n}},\hat{\mathbf{b}},\hat{\mathbf{t}}$ with $\hat{\mathbf{n}}\times\hat{\mathbf{b}} = \hat{\mathbf{t}}$, r and θ are polar coordinates in the $\hat{\mathbf{n}},\hat{\mathbf{b}}$ plane, and positive θ is measured from $\hat{\mathbf{b}}$ in the direction of $-\hat{\mathbf{n}}$. The dipole moves with a velocity u along $-\hat{\mathbf{n}}$.

In contrast to the asymptotic expansion for a single tube, useful conclusions are obtained in the case of a vortex pair from the first few orders. At zeroth order one will find just the translational velocity of the two-dimensional solution. At next order in σ/r_c there will be axial flows set up and the core area will evolve according to (2). The local volume, $\sigma^2|dr/d\xi|$, only changes at order $(\sigma/r_c)^2$.

To implement the perturbation expansion, we define a toroidal coordinate system centered on the dipole [e.g., (22)] and valid within a tube of order r_c. We consider only the restricted case where the space curve γ defined by the dipole center lies in a plane that is also the symmetry plane for the internal vorticity distribution. This plane is respected in time. It is sufficient to consider only this case in order to decide whether the singularities found in the filament models occur in the Euler equations.

Any point P_0 within a distance r_c off γ can be parametrized by toroidal coordinates (r,θ,s). The arc length s_0 measured along γ corresponding to P_0 is the intercept that a plane normal to γ must have in order to contain P_0. Within this plane we locate P_0 by polar coordinates r_0,θ_0 with positive angles θ measured from the direction of the binormal $\hat{\mathbf{b}}$ at s_0 as before. The binormal is always perpendicular to the symmetry plane mentioned above. An element of arc length is defined as

$$dP_0 = \hat{r}\,dr + r\hat{\theta}\,d\theta + h_s\hat{t}\,ds,$$

where

$$h_s = (1 + r\sin\theta/r_c) \tag{23}$$

and r_c is computed at s_0. We will occasionally use a Lagrangian coordinate ξ in place of s as was done in Eqs. (1a) and (1b) and use $\eta = (r,\theta,\xi)$ to denote the triple of toroidal coordinates. The unit tangent, normal, and binormal, $\hat{\mathbf{t}},\hat{\mathbf{n}},\hat{\mathbf{b}}$ all agree with their definitions in Sec. II.

It is now necessary to transform the Euler equations from a fixed Cartesian frame (coordinate $\mathbf{x}$) to the moving toroidal coordinates. Let

$$\mathbf{x} = \mathbf{F}(\eta,t) = \boldsymbol{\gamma}(\xi,t) + r(-\hat{\mathbf{n}}\sin\theta + \hat{\mathbf{b}}\cos\theta)$$

be the variable change. Then, as usual,

$$\left.\frac{\partial \mathbf{v}}{\partial t}\right|_x = \left.\frac{\partial \mathbf{v}}{\partial t}\right|_\eta - \frac{\partial \mathbf{v}}{\partial x_l}\frac{\partial F_l}{\partial t}.$$

It will be shown shortly that for the problem of interest,

$$\frac{d\boldsymbol{\gamma}}{dt} = -u(s,t)\hat{\mathbf{n}}. \tag{24}$$

[This equation essentially defines u since $d\boldsymbol{\gamma}/dt$ must be orthogonal to $\hat{\mathbf{b}}$. Contributions parallel to $\hat{\mathbf{t}}$ appear at $O(\epsilon^2)$ and are not simply unphysical reparametrizations of $\boldsymbol{\gamma}$ since (2) keeps track of the local stretching in terms of σ.] Then

$$\partial_t \mathbf{v}|_x = \partial_t \mathbf{v}|_\eta + \left(u\hat{\mathbf{n}} + r\frac{\partial u}{\partial s}\sin\theta\hat{\mathbf{t}}\right)\cdot\partial_x \mathbf{v}. \tag{25}$$

Note also

$$\partial_t \hat{\mathbf{r}} = \hat{\mathbf{t}}\,\partial_s u\sin\theta, \quad \partial_t\hat{\boldsymbol{\theta}} = \hat{\mathbf{t}}\,\partial_s u\cos\theta, \quad \partial_t\hat{\mathbf{t}} = -\hat{\mathbf{n}}\,\partial_s u.$$

The Euler equations are written

$$\begin{aligned}
&\partial_t v_r|_x + \left[\left(v_r\,\partial_r + \frac{v_\theta}{r}\partial_\theta\right)v_r - \frac{v_\theta^2}{r} + \partial_r p\right] \\
&\quad = \left(\frac{v_s^2}{r_c h_s}\sin\theta - \frac{v_s}{h_s}\partial_s v_r\right), \\
&\partial_t v_\theta|_x + \left[\left(v_r\,\partial_r + \frac{v_\theta}{r}\partial_\theta\right)v_\theta + \frac{v_r v_\theta}{r} + \frac{1}{r}\partial_\theta p\right] \\
&\quad = \left(\frac{v_s^2}{r_c h_s}\cos\theta - \frac{v_s\,\partial_s\,\partial v_\theta}{h_s}\right), \qquad (26) \\
&\partial_t v_s|_x + \left(v_r\,\partial_r + \frac{v_\theta}{r}\partial_\theta\right)v_s \\
&\quad = -\frac{\partial_s p}{h_s} - \frac{v_s}{h_s r_c}(v_r\sin\theta + v_\theta\cos\theta) - \frac{v_s}{h_s}\partial_s v_s, \\
&\frac{1}{r}\partial_r(rv_r) + \frac{1}{r}\partial_\theta v_\theta + \frac{\partial_s v_s}{h_s} + \frac{1}{r_c}(v_r\sin\theta + v_\theta\cos\theta) \\
&\quad = 0.
\end{aligned}$$

To scale these equations, let $\sigma(\xi,t)$ be the transverse dimension of the dipole [e.g., a in (22)] and $r_c(\xi,t)$ the corresponding radius of curvature of $\boldsymbol{\gamma}$. Uppercase Latin letters or Φ will henceforth denote scaled quantities. We define

$$\begin{aligned}
&R = r/\sigma, \quad dS = ds/r_c, \\
&dT_s = (\Gamma/\sigma r_c)dt, \quad dT_f = (\Gamma/\sigma^2)dt, \\
&V = \sigma v/\Gamma, \quad P = \Gamma^2 p/\sigma^2, \quad \Phi = \Gamma\phi.
\end{aligned}$$

The expansion parameter is $\epsilon \equiv \sigma/r_c$ and depends on ξ and t.

We have noted many times that the scales of variation perpendicular to $\boldsymbol{\gamma}$ and along it differ by a factor ϵ. Hence ∂_R and ∂_S are both order 1. The velocity is scaled by its characteristic value near the dipole. The velocity potential ($v = \nabla\phi$) and the pressure p are adjusted similarly. Finally we have introduced two time scales to account for the very different rates at which the dipole moves (T_f) and deforms and stretches (T_s). The scaled equations read

$$\begin{aligned}
&H_s = (1 + \epsilon R\sin\theta), \\
&\partial_{T_f} V_R|_x + \{[V_R\,\partial_R + (V_\theta/R)\partial_\theta]V_R - V_\theta^2/R + \partial_R P\} \\
&\quad = -\epsilon\{\partial_{T_s} V_R - \partial_{T_S}(\ln\sigma)(V_R + R\,\partial_R V_R) \\
&\qquad + \epsilon(\partial_{T_s} S)(\partial_S V_R) - (V_s^2/H_s)\sin\theta + (V_s/H_s) \\
&\qquad \times[\partial_s V_R - \partial_S(\ln\sigma)(V_R + R\,\partial_R V_R) \\
&\qquad + \partial_S T_f\,\partial_{T_f} V_R + \epsilon\,\partial_S T_s\,\partial_{T_s} V_R]\}, \\
&\partial_{T_f} V_\theta|_x + \left[\left(V_R\,\partial_R + \frac{V_\theta}{R}\partial_\theta\right)V_\theta + \frac{V_R V_\theta}{R} + \frac{\partial_\theta P}{R}\right] \\
&\quad = -\epsilon\Big(\partial_{T_s} V_\theta - \partial_{T_s}(\ln\sigma)(V_\theta + R\,\partial_R V_\theta) \\
&\qquad - \epsilon\,\partial_{T_s} S\,\partial_S V_\theta - \frac{V_s^2\cos\theta}{R} + \frac{V_s}{H_s} \\
&\qquad \times[\partial_s V_\theta - \partial_s(\ln\sigma)(V_\theta + R\,\partial_R V_\theta) \\
&\qquad + \partial_s T_f\,\partial_{T_f} V_\theta + \epsilon\,\partial_s T_s\,\partial_{T_s} V_\theta]\Big), \qquad (27) \\
&\partial_{T_f} V_s|_x + [V_R\,\partial_R + (V_\theta/R)\partial_\theta]V_s \\
&\quad = -\epsilon[(1/H_S)\partial_s P - 2(\partial_s\ln\sigma)P + (\partial_s T_f)(\partial_{T_f} P) \\
&\qquad + \epsilon\,\partial_s T_s(\partial_{T_s} P)] + (V_s/H_S)(V_R\sin\theta \\
&\qquad + V_\theta\cos\theta) - (V_s/H_S)[\partial_s V_s - (\partial_s\ln\sigma)V_s \\
&\qquad + \partial_s T_f\,\partial_{T_f} V_s + \epsilon\,\partial_s T_s\,\partial_{T_s} V_s] + \partial_{T_s} V_s \\
&\qquad - (\partial_{T_s}\ln\sigma)(V_s + R\,\partial_R V_s) + \epsilon(\partial_{T_s} S)\partial_s V_s, \\
&(1/R)\partial_R(RV_R) + (1/R)\partial_\theta V_\theta \\
&\quad = -(\epsilon/H_S)[\partial_s V_s - \partial_s(\ln\sigma)(V_s + R\,\partial_R V_s) \\
&\qquad + (\partial_s T_f)(\partial_{T_f} V_s) + \epsilon(\partial_s T_s)(\partial_{T_s} V_s) \\
&\qquad + (V_R\sin\theta + V_\theta\cos\theta)].
\end{aligned}$$

In regions where the vorticity is zero it is most convenient to solve Poisson's equation $\nabla^2\Phi = 0$ for the velocity potential Φ in scaled variables,

$$\begin{aligned}
&\partial_R^2\Phi + \frac{1}{R}\partial_R\Phi + \frac{1}{R^2}\partial_\theta^2\Phi \\
&\quad + \frac{\epsilon}{H_s}\left(\sin\theta\,\partial_R\Phi + \frac{\cos\theta}{R}\partial_\theta\Phi\right) + \frac{\epsilon}{H_s}\partial_s\left(\frac{\epsilon}{H_s}\partial_s\Phi\right) \\
&\quad = 0.
\end{aligned} \tag{28}$$

Since it is only initially that vorticity is confined to a circular region of radius σ, we must allow this region to change both area and shape. In toroidal coordinates, we write the boundary in polar form for each ξ as

$$r = a(\xi,\theta,t) = \sigma(\xi,t) + \epsilon a_1(\xi,\theta,t). \tag{29}$$

We are restricted to considering small ϵ and smooth dependence on θ. Finally all fields are expanded in ϵ:

$$V = V^0 + \epsilon V^1 + \epsilon^2 V^2 + \cdots .$$

We chose not to introduce any axial flow at zeroth order so that $V_s^0 = 0$.

It is physically plausible and indeed checked perturbatively, to the order in which we work, that V at fixed η, the core size, and other quantities measured with respect to γ depend on T_s only. Therefore we can use (25) to rewrite $\partial_t v|_x$ in terms of $\partial_{T_s} V|_\eta$ and a convective term. The zeroth-order equations read

$$\begin{aligned}
&-U\left(\sin\theta\,\partial_R + \frac{\cos\theta}{R}\partial_\theta\right)V_R^0 + \left(V_R^0\,\partial_R + \frac{V_\theta^0}{R}\partial_\theta\right)V_R^0 \\
&\quad - \frac{V_\theta^{02}}{R} + \partial_R P^0 = 0, \\
&-U\left(\sin\theta\,\partial_R + \frac{\cos\theta}{R}\partial_\theta\right)V_\theta^0 + \left(V_R^0\,\partial_R + \frac{V_\theta^0}{R}\partial_\theta\right)V_\theta^0 \\
&\quad + \frac{V_R^0 V_\theta^0}{R} + \frac{1}{R}\partial_\theta P^0 = 0, \\
&\partial_R(RV_R^0) + \partial_\theta V_\theta^0 = 0,
\end{aligned} \tag{30}$$

where $U = \sigma u/\Gamma$ appears in the scaled version of (25). These equations are then satisfied by any two-dimensional dipole moving with velocity U. Thus to zeroth order in ϵ, each slice through the three-dimensional dipole tube moves independently with a velocity U as we anticipated above in (24). This form also agrees with the local model equations when ρ and σ are frozen, which they are at this order.

To next order in ϵ we linearize the left-hand sides of (27) and substitute V^0, etc., onto the right-hand sides. The solution has to be constructed separately in several regions and then matched. We define

$$\begin{aligned}
&0 \leqslant r \leqslant a, && \text{interior,} \\
&a \leqslant r < r_c, && \text{inner,} \\
&a \ll r < \infty, && \text{outer.}
\end{aligned} \tag{31}$$

The two regions $r \geqslant a$ may be collectively called exterior. All vorticity is confined to the interior region [cf. (22)]. The breakdown of the toroidal coordinate system for $r \sim r_c$ forces one to distinguish the "inner" and "outer" regions. Note that since $a/r_c \sim \sigma/r_c \ll 1$, there is a substantial region of overlap between them on which the respective asymptotic expansions must match.

We will work from $r = \infty$ inwards. Clearly in the exterior region it suffices to solve just the Poisson equation (28) with an interior boundary condition defined at $r = a$. The full Euler equations (27) are only needed for $r < a$.

In the outer region for $r \gg a$ or $R \gg 1$, we can perform the analog of a multipole expansion in electrostatics for the potential due to a distant charge distribution. The outer solution is only needed to determine the boundary conditions on the inner solution so we will impose the additional restriction $r \ll r_c$. Examination of the general integral formula for ϕ in terms of ω indicates that we can approximate the distributed dipole centered on γ by a pair of antiparallel circular filaments separated by ρ. At fixed s the potential reads

$$\begin{aligned}
\phi(a \ll r \ll r_c) &= \frac{1}{2\pi}\int \mathbf{r}' \times \boldsymbol{\omega}(\eta,t)\, d^2 r' \cdot \nabla \ln r \\
&\quad + O\left(\frac{\Gamma\sigma^2}{r^2}, \frac{\Gamma\sigma}{r^2}\right).
\end{aligned}$$

The dipole moment of the tube at the point in question is defined to be $\Gamma\rho(\xi,t)$. The final result is

$$\begin{aligned}
\phi(r,\theta,\xi) &= \frac{\Gamma\rho}{2\pi r}\sin\theta \\
&\quad + \frac{\Gamma\rho}{4\pi r_c}\left[\ln\left(\frac{8r_c}{r}\right) - \cos^2\theta\right] + O\left(\frac{\Gamma\rho r}{r_c^2}\right),
\end{aligned} \tag{32}$$

when $r/r_c \to 0$.

In the inner region we have to work from a general solution to the Laplace equation (28). The first two orders read ($\Phi = \Phi_0 + \epsilon\Phi_1 + \cdots$)

$$\partial_R^2\Phi_0 + (1/R)\partial_R\Phi_0 + (1/R^2)\partial_\theta^2\Phi_0 = 0, \tag{33a}$$

$$\begin{aligned}
&\partial_R^2\Phi_1 + \frac{1}{R}\partial_R\Phi_1 + \frac{1}{R^2}\partial_{\theta^2}\Phi_1 \\
&\quad + \left(\sin\theta\,\partial_R\Phi_0 + \frac{\cos\theta}{R}\partial_\theta\Phi_0\right) = 0.
\end{aligned} \tag{33b}$$

We can rederive our solution (22)–(30) for $r > a$ by solving the two-dimensional Laplacian (33a) with $\Phi_0 = U\sin\theta/R$. The value of ρ can be calculated from the interior solution at zeroth order,

$$\Gamma\boldsymbol{\rho} = \int (\mathbf{x}\omega_s)\, d^2 x.$$

We can therefore match Φ^0 to the first term in (32) by setting

$$\Gamma\rho/2\pi = \Gamma U\sigma = u\sigma^2.$$

To account for the remaining terms in (32), we write out a general solution to (33b) with the inhomogeneous terms and match to (32). One finds

$$\begin{aligned}
\Phi_1 &= \frac{U}{2}\left[\ln\left(\frac{8}{\epsilon R}\right) + \frac{\cos(2\theta)}{2}\right] \\
&\quad + \sum_{n=1}^{\infty}\frac{c_n\cos(n\theta) + d_n\sin(n\theta)}{R^n}.
\end{aligned} \tag{34}$$

The c_n, d_n are fixed at the interior–exterior boundary, i.e., by imposing that the boundary of the vortex tube move with the fluid; symbolically,

$$\left(\frac{\partial}{\partial t} + \mathbf{v}\cdot\nabla\right)[r - a(\xi,\theta,t)] = 0. \tag{35}$$

When Eq. (35) is expanded to $O(\epsilon)$ one finds

$$\begin{aligned}
\partial_R\Phi_1|_{R=1} &= -\partial_R^2\Phi_0\frac{a_1}{\sigma} + \partial_{T_s}\ln\sigma \\
&\quad + U\cos\theta\frac{\partial_\theta a_1}{\sigma} + \partial_\theta\Phi_0\frac{\partial_\theta a_1}{\sigma}.
\end{aligned} \tag{36}$$

By explicitly substituting Φ_0 into (36) one finds that the angular average of $\partial\Phi_1/\partial R$ is just $\partial\ln\sigma/\partial T_s$.

Now recalling the form of Φ, compatible with the outer boundary condition (34), we find

$$\frac{\partial\ln\sigma}{\partial T_s} = -\frac{U}{2} \tag{37a}$$

or

$$\frac{\partial(\sigma^2|\partial_\xi \gamma|)}{\partial T_s} = O(\epsilon). \tag{37b}$$

We have used (24) [cf. (15)] to derive an equation for $|\partial_\xi \gamma|$. (The stretching is simply a consequence of the form of the equation for $d\gamma/dt$.) The formula for local volume conservation (2) we used in our models has been derived to the indicated order. The remaining unknown angular-dependent term in Φ may be expressed in terms of the Fourier series for a_1. Since γ is a plane curve and the vorticity distribution is symmetric the terms in a_1 and ϕ_1 proportional to $\cos[(2n+1)\theta]$ and $\sin(2n'\theta)$ vanish. The velocity field just outside the core, neglecting a_1, is just

$$v_r^1 = -\frac{\Gamma\rho}{4\pi r_c} r^{-1}, \quad v_\theta^1 = \frac{\Gamma\rho}{4\pi r_c}\frac{\sin 2\theta}{r}.$$

In more formal language, the radial term forces us to choose a σ obeying (37b) and therefore (37a) is a solvability condition for (36). The existence of the quadrupolar term in the θ direction does not lead to any solvability condition at this order and merely becomes a boundary condition that we must impose on the Euler equations in the interior.

Since we imagine that $a_1 = 0$, initially its value at later times is undetermined to this order since it is only a function of T_s and $\partial a_1/\partial T_s$ enters (35) at $O(\epsilon^2)$. We can also solve for the interior flow with $a_1 \neq 0$ as a boundary condition. We are uncertain whether a solvability condition for the deformation exists at higher order.[34]

The interior solutions[25] can be reduced to a set of third-order differential equations for the radial dependence of each Fourier mode in θ. We merely state the angular dependences of the corrections to V^0, which may be read off from the inhomogeneous terms and boundary conditions. The ambiguities in overall sign are settled by reference to direct numerical simulations of the three-dimensional Euler equations to be published elsewhere.

The vorticity component parallel to $\hat{\mathbf{t}}$ varies as $\sin 2\theta$. Since $\omega_0 \propto -\cos\theta$, $|\omega_0 + \epsilon\omega_1|$ is enhanced with respect to $|\omega_0|$ on the side of the dipole in the direction of propagation (Fig. 16). The θ dependence of ω^1 is simply the signature for $r < a$ of the quadrupolar term in v' we found outside the core [Eq. (34)].

The velocity component parallel to $\hat{t}$ varies like $\sin\theta\, d\sigma/ds$. The sign of the axial flow can be inferred by recalling that within the local model the two filaments are pushed together at a rate proportional to r_c^{-1}. When the positive core size is taken into account, the back of the tube has a smaller radius of curvature than the front, so one expects fluid to be squeezed out from the back. The interior average axial velocity (denoted by an overbar) is zero to order ϵ since we expect an equation of the form

$$\frac{\partial}{\partial T_s}(\sigma^2 \partial_\xi s) + \frac{\partial}{\partial \xi}(\overline{\mathbf{v}\cdot\mathbf{t}}\sigma^2) = 0$$

to hold. Then (37) implies $\overline{\mathbf{v}\cdot\mathbf{t}} = O(\epsilon^2)$.

B. Navier–Stokes equations

It has not been ruled out that the core deformation in successive orders of perturbation theory behaves as $(\epsilon T_s)^n$,

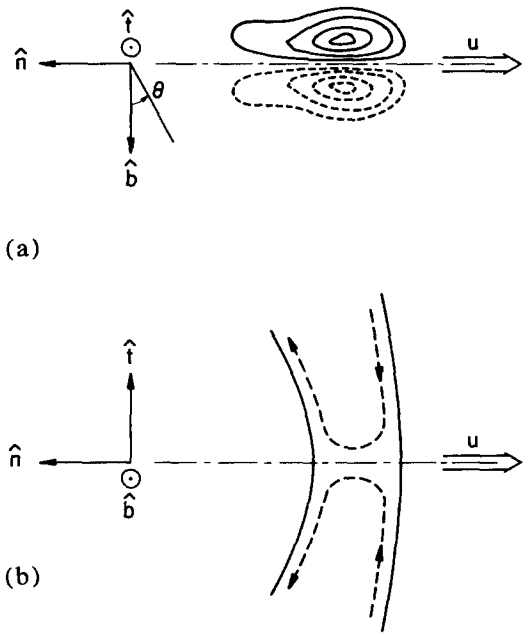

FIG. 16. (a) The shape changes an initially circular vortex core is apt to undergo when the filament stretches. Positive and negative vorticity contours are shown as well as our conventions for the axis and θ. In (b) the dominant axial flows (dashed) are shown around the point of maximum stretching. The paired filament moves in the direction indicated by u.

so that the expansion in Sec. IV A ceases to be valid beyond a certain scaled time and all connection with the filament solutions is lost. Nevertheless, in this section the deformation will be assumed bounded up until the singularity time in order to show that viscous effects are ineffective in halting the collapse. In the simplest possible terms, the time on which the viscosity ν acts to cancel out and diffuse the vorticity in the core is σ^2/ν and thus is always much less than the time remaining until the singularity [N.B. Eq. (19)].

To argue more formally, consider the rescaled times given above (27) in integrated form

$$T_f = [t^*\Gamma/\sigma^2(0)]\,|\ln(1 - t/t^*)|, \quad T_s = \epsilon T_f, \tag{38}$$

where we used in an essential way (37a) in unscaled form,

$$\sigma^2(t) \sim \epsilon\Gamma(t^* - t) = \sigma^2(0)(1 - t/t^*).$$

The $\sim$ sign represents numerical factors of order 1 and $t = 0$ in the second equality can be replaced by any time within the self-similar regime. The original interval $0 < t < t^*$ has been stretched out into $0 \leqslant T_{s,f} < \infty$. (The logarithms in σ that occurred in the local model of Sec. II C have been neglected.) Our assumption now becomes, in the notation of (27), that $\mathbf{V}(\mathbf{R}, S, T_f, T_s)$ is a fixed form solution to the scaled Euler equations for all $T_{f,s} > 0$.

The scaled Navier–Stokes equations read

$$\partial_{T_f} V + V\cdot\nabla V + \epsilon H(V) = -\nabla P + (\nu/\Gamma)\nabla^2 V,$$

where H represents the $O(\epsilon)$ terms in (27) and $\nu/\Gamma \ll 1$. One can now change to a comoving toroidal coordinate system and equate orders in ϵ as before. The viscous term breaks up into an order ϵ^0 two-dimensional piece in (R,θ) and $O(\epsilon)$ terms involving the axial dependence. The zeroth-order

equation is just the two-dimensional Navier–Stokes equations in which all the coordinates are scaled.

There are no exact analytic vortex dipole solutions in the presence of viscosity, but the behavior of a solution such as (22) when a small amount of viscosity is added for $\nu T_f/\Gamma \ll 1$ can safely be predicted. Vorticity diffusing across the neutral streamline down the center of the dipole will cause the circulation in each half to decay as $(1-\nu T_f/\Gamma)$. A wake will also be created by vorticity leaving the circumference of the dipole as it translates. The integral of the magnitude of the vorticity across the wake is of order ν/a. We do not believe there are any instabilities and that for $\nu T_f/\Gamma \geqslant 1$ the dipole simply diffuses away. Even with instabilities, we do not see how the dissipation could modify the Euler solutions for $\nu T_f/\Gamma \ll 1$ since all gradients are order 1 and there are no rigid boundaries.

Since the two-dimensional limit is unaffected by viscosity and the full Euler solutions exist we presume the perturbation theory continues to work with viscosity for short times, $\nu T_f/\Gamma \ll 1$. We can therefore trust the Euler solutions until $T_f \sim \Gamma/\nu$ or

$$\sigma(t) \sim \exp(-\epsilon \,\mathrm{cst}\, \Gamma/\nu).$$

Note that Γ/ν plays the role of a Reynolds number and must be much greater than 1 for everything said so far to make qualitative sense. The velocity and vorticity scale as Γ/σ, Γ/σ^2, respectively. In practical terms, this viscosity cannot prevent σ from getting so small (and $\max|v|$ so large) that hydrodynamics is inapplicable.

It would clearly be of interest to rigorously prove that the Euler and Navier–Stokes solutions remain close under the conditions we are considering. Crude estimates do exist for the unscaled equations but they work by bounding how rapidly the difference velocity can grow in time.[35] Clearly if the Euler solution is unstable, the viscous perturbation may excite the unstable modes and lead to an order 1 difference for $T_f \sim \ln(\Gamma/\nu)$. Arguments of this sort tend to be unnecessarily pessimistic since small changes in velocity will ultimately cause two solutions to differ even if they are identical when brought into coincidence. Also our zeroth-order solutions are stable and ultimately we are only concerned with existence and not stability. Nevertheless a strong enough comparison theorem between Navier–Stokes and Euler solutions seems difficult to prove.

V. CONCLUSION

It is our contention that singular, though possibly unstable, solutions to the Navier–Stokes equations in three dimensions cannot be dismissed without serious consideration. Our arguments in their favor have utilized a variety of models and techniques so we will recapitulate our reasoning and justify the significant approximations. We begin with a synopsis of the rigorous constraints that have been placed on singular solutions to Navier–Stokes.

A. Rigorous results

Leray was the first mathematician to seriously attack the question of whether solutions to the Navier–Stokes equations exist and are unique.[1] It suffices to consider a smooth initial velocity field, confined to a finite box B with no slip boundary conditions and no external forces. Then Leray showed the following ("cst" will denote free unrelated constants).

(i) There exists a unique smooth solution for a finite interval of time for any viscosity and a solution for all times if the viscosity is sufficiently large.

(ii) If the solution is not smooth at a time t^*, then for any $t < t^*$ and after the last singularity,

$$\max_{x\in B}|v(x,t)| \geqslant \mathrm{cst}_1[\nu/(t^*-t)]^{1/2},$$
$$\int_B |\nabla v|^2\, d^3x \geqslant \mathrm{cst}_2\left(\frac{\nu^3}{(t^*-t)}\right)^{1/2}, \tag{39}$$

where the cst_i are pure numbers [i.e., independent of $v(x,0)$].

(iii) A so-called "weak solution" may be defined in analogy to a δ function by multiplying the Navier–Stokes equation by an arbitrary smooth test function and integrating. The weak solutions may be nonunique but exist for all times and permit one to continue through the singularity times.

Serrin[4] has sharpened result (ii) by showing that if v is a bounded solution then it is infinitely differentiable. Hence singularities, if they occur, cannot hide and the velocity cannot develop a singularity in a high derivative but must itself diverge.

The inequalities (39) are established by constructing a formal iterative solution to Navier–Stokes by inverting the linear part of the equations for the ith iterate onto the nonlinear terms for the $(i-1)$th iterate. If $|\mathbf{v}|$ is bounded, then the iteration converges and a smooth solution emerges. The various powers in (39) are just what one would infer dimensionally.

Scheffer,[5] following Leray, bounded the Hausdorff dimension of the set of singular times by 0.5. Since the total dissipation cannot exceed the initial energy,

$$\nu\int_0^\infty \int_B |\nabla v|^2\, dt\, d^3x \leqslant \int_B |v(x,0)|^2\, d^3x.$$

But for each t_i^*, (39) holds for $t_i^* > t > t_{i-1}^*$. Hence the sum of cst $\nu^{5/2}(t_i^* - t_{i-1}^*)^{1/2}$ over all singular times is bounded by the energy. A bound on the covering of the set of singular times follows along with the Hausdorff dimension.

Subsequent authors have extended Leray's results by considering the singularity as a space-time event.[6] The distance from a singularity at t^*, x^* is measured by

$$r^2 = (x-x^*)^2 + \nu(t^*-t),$$

with $t \leqslant t^*$. Then in the neighborhood of a singularity, (39) generalizes to

$$|v(x,t)| > \mathrm{cst}_1/r,$$
$$\int_{\substack{0<t^*-t<r \\ |x-x^*|<r}} |\nabla v|^2 > \mathrm{cst}_2\, r,$$

and in addition

$$|\nabla v| > \mathrm{cst}/r.$$

The inequality on the dimension of the singular times becomes the statement that when we cover the singular set

by rectangles of size ϵ^2 in t and ϵ in x, then the Hausdorff dimension is less than 1. Therefore the singular set can be just smaller than a space curve at one time or pointlike in space on a set of times with ordinary Hausdorff dimension less than one half.

An interesting generalization of these results is obtained by considering a modified version of the Navier–Stokes equations with the dissipation replaced by $\tilde{\nu}(-\nabla^2)^{1+\epsilon}v$.[36] Then on dimensional grounds the inequality analogous to (39) reads[6]

$$\tilde{\nu}\int_B v(-\nabla^2)^{1+\epsilon}v\,d^3x > \text{cst}\,\tilde{\nu}^{5/(2+2\epsilon)}(t^*-t)^{-(1+6\epsilon)/(2+2\epsilon)}.$$

The time singularity on the right does not have a finite integral for $\epsilon > \frac{1}{4}$. Hence by the energy argument, there are no singularities for $\epsilon > \frac{1}{4}$ since the integrated dissipation would exceed the initial energy.

B. Summary

Let us for the moment ignore logarithmic terms. Then the Biot–Savart model with local volume conservation implies that vortex filaments will pair in an antiparallel manner and generate infinite stretching or zero core size in a finite time. The ratio of filament spacing to core size remains fixed and σ tends to zero as $(t^*-t)^{1/2}$. There are solutions (cf. Sec. III B) for which σ/r_c remains small so it is sensible to think of the filament as the limit of a nonzero core vortex solution of the Euler equations. The numerical simulations and the analytic results for local approximations to Biot–Savart establish these conclusions unambiguously.

For short periods of time, a solution to the full Euler equations for paired vortex tubes exists that follows the filament solutions. If the vortex tubes do not deform significantly, then we expect they will continue to track the filament solutions. The inequality $\sigma/r_c \ll 1$ makes the self-stretching appear on the scale of σ as simply a rescaling.

The time for viscous effects to enter is σ^2/ν, which for small viscosity ν greatly exceeds the time remaining to the singularity, (t^*-t). Therefore the viscous diffusion will not halt the collapse until $\sigma \sim \exp(-\text{cst}\,\Gamma\epsilon/\nu)$, Sec. IV B.

We consider there to be three significant assumptions in the above train of argument. The most serious, and the one we cannot justify, is the neglect of secular distortions when paired vortex tubes self-stretch under the Euler equations. Limited spectral simulations have suggested that the tubes flatten into a pair of ribbons that then behave very differently from a pair of vortex filaments.[31] The most crucial step in generating singular solutions to Navier–Stokes is in fact constructing their counterparts with $\nu = 0$. The two other assumptions that we consider reasonable, namely the neglect of dynamics in the vortex cores and the absence of a conserved energy for filament models, are considered below.

We believe that whenever one has a solution to the Euler equations that is smooth and contains a single spatial scale when written in terms of $x/\sqrt{t^*-t}$, then a similar solution to the Navier–Stokes equation exists as long as $|\ln(t^*-t)|/R^\alpha \ll 1$, where R is the Reynolds number and $\alpha > 0$ is a power we are unable to calculate. A partial argument for paired filaments was given in Sec. IV B. The reason an exponent 1/2 appears in the Euler equation [e.g., $\sigma \sim (t^*-t)^{1/2}$] at least for filaments is ultimately dimensional; Γ is the only relevant conserved dimensional quantity.

It is informative to give a physical restatement of the scaling analysis of Sec. IV B which also suggests why paired vortex tubes are the most logical candidate for a singular solution. In the presence of viscosity we rewrite (2) as

$$\frac{d\sigma^2}{dt} = \nu - \sigma^2\frac{d\ln(\partial_\xi s)}{dt}. \tag{40}$$

The logarithmic derivative in the second term is just the rate of strain along the tangent to the filament. It can be estimated as a velocity gradient $\sim \text{cst}\,\Gamma/[\max(\rho,\sigma)r_c]$. The factor r_c enters since straight filaments do not stretch and the gradient along the filament involves r_c^{-1}. Therefore it is only because $\sigma^2/(\rho r_c)$ is time independent near t^* that $d\sigma^2/dt$ can be negative, and σ^2 can hit zero. We are not able to devise another flow involving vortex sheets or ribbons in which the velocity and rate of strain scale as Γ/σ and Γ/σ^2, respectively.

At the level of (40), we can also give an account of why changing the dissipation function to $-\tilde{\nu}(-\nabla^2)^{1+\epsilon}$ controls the singularity. On dimensional grounds,

$$\frac{d\sigma^2}{dt} = -\frac{\tilde{\nu}}{\sigma^{2\epsilon}} - \frac{\text{cst}\,\Gamma\sigma^2}{\max(\rho,\sigma)\cdot r_c}.$$

Therefore σ^2 always has a nonzero positive fixed point. The rigorous results that currently exist only demonstrate existence and regularity for $\epsilon > \frac{1}{4}$. We conjecture any $\epsilon > 0$ guarantees smooth solutions exist for all times. Thus the usual Laplacian dampening term is "marginal" with respect to controlling singularities. While we expect in any real fluid that $\tilde{\nu}\nabla^4$ dissipation terms exist, the ratio $\tilde{\nu}/\nu$ will be of order an interparticle spacing squared. Hence singularities could reach atomic scales before being damped.

Logarithms frequently enter problems in which two distinct physical effects just manage to balance. Here we found that $(\rho/\sigma)^2 \sim 1/\ln(\sigma^{-1})$ so that eventually a paired vortex filament model becomes internally inconsistent. On a similar scale, the viscosity would reduce the circulation to zero. Clearly σ can get very small, and the velocity or vorticity, $(\Gamma/\sigma, \Gamma/\sigma^2)$, very large, before $\ln(\sigma^{-1})$ is appreciable.

Our model for singularities in the Navier–Stokes equations works only because the two-dimensional numbers in the problem, viscosity and circulation, have the same units. Leray[1] proved that the velocity is smooth unless $\max|v| > \text{cst}[\nu/(t^*-t)]^{1/2}$. We found the same exponent since we have $\sigma^2 \sim \text{cst}\,\Gamma(t^*-t)$. It is worth noting that had we found a larger exponent, i.e., $\sigma^2 \sim (t^*-t)^\alpha$, $\alpha > 1$, then the rigorous lower bound would be satisfied near t^* but it would no longer be physically reasonable to consider the viscosity as a small perturbation. That is, $\sigma^2/\nu \ll t^*-t$, so viscosity will dissipate the circulation before the singularity is attained. Conversely, if for the Euler equations we found a smaller exponent, then the stretching would not balance the dissipation.

The correspondence between our model solutions and rigorous results is close in yet another way. For technical reasons the mathematicians view the singular set as a subset

of space-time and derive an upper bound for its Hausdorff dimension.[6] For our model this is natural since different regions along the paired filament collapse independently and each one has its own t^*.

Last we reemphasize our inability to demonstrate that vortex tubes behave like filaments when they pair and stretch. The question of singularities therefore hinges on a delicate problem in fluid mechanics and we doubt that rigorous methods will make much more progress unless they exploit more subtle aspects of the Navier–Stokes equations than the energy conservation property of the nonlinear term and a mere counting of the factors that enter it.

C. Limitations of filament models

1. Energy conservation

It was remarked below Eq. (1) that there is no conserved energy associated with a vortex filament when the core varies in time. This is not surprising since the swirling and axial flows within the core are not accounted for. The Biot–Savart model may still correctly describe how a vortex tube evolves even though details of the interior flow are lost and the energy is not a function of just the filament position and core size. Lack of manifest energy conservation makes the connection between filaments and real vortex tubes problematical if one supposes that paired tubes stretch without change in shape. Then (cf. end of Sec. II B) the energy computed from the Euler equations scales as the total length of filament L.

For this reason we were careful to show that for the local model, L goes as cst $-\sqrt{t^*-t}$ near the singularity. Nevertheless it is not obvious that energy can be transferred into some small ball around the singularity fast enough so that a cusp can develop in L with no shape change locally. (The pairing makes the energy a local function of ξ or arc length.)

To analyze this problem we have found it productive to generalize the class of flow fields we consider. Recall for the paired filaments that the dynamics was local in arc length and that a section of filament several times r_c in length should behave independently of other similar pieces. Now all lengths scale as $(t^*-t)^{1/2}$, so imagine making the ansatz that we search for a solution to the Euler equations in the form,

$$v_{ss}(x,t) = (1/\sqrt{t^*-t}) \times V(X = x/\sqrt{t^*-t},\ T = -\ln(1-t/t^*)),$$

for $x \ll 1$ and $X \gg 1$. Clearly v_{ss} has to be matched to a smooth background flow for $x \leqslant O(1)$. The total energy in v_{ss}, where it applies, is just $(t^*-t)^{1/2}$, so energy conservation no longer appears to be such a problem. By searching for T independent solutions to the Euler equations, one might be able to argue for singularities without the intermediary step of filament models. We still conjecture, however, that the continuum solution would have the symmetry as a filament pair.

2. Core dynamics

Imagine a straight axisymmetric vortex tube with a slowly varying core size. If the initial amplitude of the perturbation is sufficiently small and there are no axial flows, its subsequent evolution is described by the Korteweg–de Vries equation.[21] Larger perturbations and axial flows can lead to a jump in $\sigma(\xi)$ or even vortex breakdown.[21] In any case, if a vortex filament is evolving slowly on a time scale of $2\pi\sigma^2/\Gamma$ it is unreasonable to fix σ^2 with the local stretching as Eq. (2), since there are faster processes which redistribute area along the filament.

A phenomenological filament model incorporating certain of these features has recently been derived by Lundgren and Ashurst. They modified the Moore and Saffman equations in an *ad hoc* way by retaining a term proportional to the derivative of the tube area with respect to arc length. Its effect is to smooth out nonuniformities in the core size σ while maintaining the assumption of axisymmetry. The derivation of the Biot–Savart formula in Ref. 18 assumes, correctly for that problem, a time scale of order r_c^2/Γ and then also assumes that on such times σ becomes uniform. The Lundgren–Ashurst equations are incorrect for an axisymmetric jet and a vortex ring with axial flow.[37] However, once the pairing and stretching begin the core and filament motions occur at comparable rates and Ref. 23 may well capture the essential physics. In particular, they also found that filaments will pair and collapse with the minimum core size obeying $\sigma_{\min}^2 \sim (t^*-t)$. As a function of arc length, σ remained within 50% of its minimum for an interval $\Delta s \sim 30_{\sigma\,\min}$ long around $\sigma_{\min}$. However, there may be a kink on one side of singularity which we never found for the Biot–Savart equations. They note that the stretching appears too rapid for the axial flow to significantly redistribute the core volume.

Similar conclusions can be reached from our data but are less convincing since we can only estimate qualitatively how rapidly axial flows build up. The crudest argument is simply to take the maximum axial velocity to be $\Gamma/2\pi\sigma$ and compare its time integral to the arc length over which $\sigma \sim \sigma_{\min}$, i.e., $\Delta s \sim 100\sigma_{\min}$ (Sec. III A). If the time interval, $t_2 - t_1$, is such that $t^* - t_2 = (t^* - t_1)/2$, then $\int_1^2 (\Gamma/2\pi\sigma)dt/\sigma \sim 20$–$50$, which is not significantly less than $\Delta s/\sigma_{\min}$. A more refined argument computes the velocity actually developed by an axial pressure gradient corresponding to a pressure drop of $\sim(\Gamma/2\pi\sigma)^2$ over a length Δs. The velocity never reaches $\Gamma/(2\pi\sigma)$ and the actual distance traversed is much less than before. Hence local core volume conservation is a reasonable approximation provided the tubes remain nearly circular.

One clearly cannot assess whether the vortex cores will progressively distort and become more ribbonlike without solving the full Euler equations. The issue of vortex reconnection in the Navier–Stokes equations for $\nu/\Gamma \ll 1$ only has to be faced after one has seen infinite gradients in the Euler solutions. It was emphasized in Ref. 31 that if gradients are bounded the high Reynolds number limit of solutions to the Navier–Stokes equations approach inviscid solutions for which reconnection is impossible. Hence the simulations of Meiron and Ashurst, which reported reconnection and no distortion, were simply too viscous, which is not surprising since they were finite difference on a 32^3 lattice.[38]

Reference 31 reports higher resolution simulations, 64^3 spectral, that evidence distortion and moderate stretching.

Similar distortion is apparent in laboratory photos of Oshima and Asaka.[39] For a number of reasons detailed in Ref. 31, these simulations do not rule out singular pointlike solutions to the Euler equations which asymptotically resemble a vortex pair. A more refined code that permits one to continuously magnify the region around the singularity should yield more definitive results.

D. Experimental implications

Searching for a pointlike singularity that occurs for a brief and unknown time seems like a hopeless task. It is therefore useful to recall several experimental facts about turbulent boundary layers which are suggestive of the types of singularities our models predict. The similarity may be coincidental, but it provides a definite context in which to ask if singularities do occur, how would one see them. We will use the term "singularity" even though instabilities or core deformations may intervene before the ultimate cutoff of atomic scales or cavitation is reached. Singularities could be a useful idealization if the real flows look similar and the maximum velocity and its gradients are larger than can otherwise be accounted for.

Recall that even though the mean velocity profile in a turbulent boundary layer is accurately described by simple scaling ideas,[7] a finite fraction of the Reynolds stress is produced by "bursts" in which the velocity gradients fluctuate to 10–20 times their value in the mean flow.[10] There is considerable experimental evidence that paired antiparallel vortex tubes are continuously formed in a turbulent boundary layer.[12] Further observations and several phenomenological models link the bursts to a breakdown of the hairpins.[40]

Experiments and numerical simulation show the hairpins to be oriented around a 45° angle with the wall which is precisely the direction in which the vortex tubes extract maximum energy from the mean flow by stretching.[12–14] An unanswered, and in our view key, question is the ratio of the tube vorticity to the strain rate of the mean flow. It has generally been assumed that the hairpin passively stretches in the mean flow. Within a singularity model, once the internal vorticity exceeds the background, the mean flow becomes irrelevant and self-stretching is alone sufficient, and indeed necessary, to cause singularities. One should be able to extract from experiment the residence time of the hairpin and the associated strain and thereby compute the vorticity expected from a passive stretching model.

Inflection points are considered a typical mode of instability for nearly inviscid shear flows.[41] More specifically, the Rayleigh criterion for inviscid plane parallel flows requires a channel that is sufficiently wide, and the spanwise vorticity to be a local maximum at the inflection. What happens for later times if the flow is constrained to be two dimensional? By analogy with the Kelvin–Helmholtz singularity, which has been followed for long times numerically,[42] we expect the vorticity to roll up into blobs that approximately fill the channel. This is not a particularly violent or rapid instability any more than it is for the mixing layer. Of course what happens in reality is that spanwise fluctuations in the vortex tubes produced by the two-dimensional rollup get rapidly amplified by the mean flow. This scenario is just the conventional argument for how hairpins are produced from the spanwise vorticity created viscously at the wall. We consider "hairpin" to be as generic a mode of instability for shear flows as inflection points are in the mean flow. With this observation, the occasional speculation that hairpins burst when the local mean flow develops an inflection translates into the supposition that big hairpins grow smaller hairpins. This may be nothing other than a paired filament singularity.

ACKNOWLEDGMENTS

The authors have profited from discussions with the Cornell SRO study group on turbulent boundary layers. R. Kerr kindly provided us with a code suitable for simulating the three-dimensional Navier–Stokes equations. We thank the authors of Refs. 23 and 29 for communicating their results prior to publication and for discussions.

Our research was supported in part by a grant from the U.S. Department of Energy (Grant No. AC02-83ER13044), the Office of Naval Research (SRO IV Fluid Mechanics Program Code 432F), and the National Science Foundation (Grant No. DMR 8314625).

[1] J. Leray, Acta Math. **63**, 193 (1934).
[2] J. L. Lions, *Quelques Méthodes de Resolution des Problèmes aux Limites Non linéaires* (Gauthier-Villars, Paris, 1969), p. 466.
[3] R. Témam, *Navier–Stokes Equations* (North-Holland, Amsterdam, 1979).
[4] J. Serrin, Arch. Rat. Mech. Anal. **9**, 187 (1962).
[5] V. Scheffer, in *Turbulence and Navier Stokes Equation, Lecture Notes in Mathematics*, Vol. 565, edited by A. Dold and B. Eckmann (Springer, New York, 1976), p. 174; V. Scheffer, Commun. Math. Phys. **61**, 41 (1978).
[6] L. Caffarelli, R. Kohn, and L. Nirenberg, Commun. Pure Appl. Math. **35**, 771 (1982).
[7] L. D. Landau and E. M. Lifshitz, *Fluid Mechanics* (Pergamon, London, 1959), Chap. 3.
[8] M. Brachet, D. Meiron, B. Nickel, S. Orszag, and U. Frisch, J. Fluid Mech. **130**, 411 (1983).
[9] A. J. Chorin, Commun. Math Phys. **83**, 517 (1982).
[10] W. Willmarth and T. Bogar, Phys. Fluids **20**, S9 (1977).
[11] S. Kline, W. Reynolds, F. Schraub, and P. Runstadler, J. Fluid Mech. **30**, 741 (1967).
[12] M. Head and P. Bandyopadhyay, J. Fluid Mech. **107**, 297 (1981).
[13] J. Kim and P. Moin, J. Fluid Mech. **162**, 339 (1986).
[14] J. Kim, Phys. Fluids **28**, 52 (1985).
[15] M. Melander, E. Overman, and N. Zabusky, submitted to Appl. Numer. Math.
[16] E. D. Siggia, Phys. Fluids **28**, 794 (1985).
[17] E. D. Siggia and A. Pumir, Phys. Rev. Lett. **55**, 1749 (1985).
[18] D. Moore and P. Saffman, Philos. Trans. R. Soc. London Ser. A **272**, 403 (1972).
[19] A. Leonard, Annu. Rev. Fluid Mech. **17**, 523 (1985).
[20] S. Widnall and D. Bliss, J. Fluid Mech. **50**, 335 (1971).
[21] S. Leibovich, Annu. Rev. Fluid Mech. **10**, 221 (1978).
[22] D. Moore and P. Saffman, Proc. R. Soc. London Ser. A **346**, 413 (1975).
[23] T. Lundgren and W. Ashurst, submitted to J. Fluid Mech.
[24] S. C. Crow, AIAA J. **8**, 2172 (1970).
[25] S. E. Widnall, D. Bliss, and A. Zalay, *Aircraft Wake Turbulence and its Detection*, edited by J. Olsen (Plenum, New York, 1971), p. 305.
[26] S. Widnall, D. Bliss, and C. Tsai, J. Fluid Mech. **66**, 35 (1974).
[27] P. G. Saffman, J. Fluid Mech. **84**, 625 (1978).
[28] G. K. Batchelor, *Introduction to Fluid Mechanics* (Cambridge U.P., New York, 1967), Chap. 7.
[29] A. Leonard, K. Shariff, and N. Zabusky (private communication).
[30] P. Moin, A. Leonard, and J. Kim, Phys. Fluids **29**, 955 (1986).
[31] A. Pumir and R. Kerr, Phys. Rev. Lett. **58**, 1636 (1987).

[32]H. Aref and E. D. Siggia, J. Fluid Mech. **109**, 435 (1981).
[33]See Ref. 27, p. 535.
[34]Our remark in Ref. 17 that the inviscid deformation could be bounded until $\sigma(t)/\sigma(0) \sim \exp(-\epsilon^{-1/2})$ is incorrect.
[35]P. Constantin, Commun. Math. Phys. **104**, 311 (1986).
[36]See Ref. 2, p. 97.
[37]As a general remark, the equation derived by Lundgren and Ashurst does not depend in any way on the actual distribution of vorticity and axial velocity inside the core. This contradicts several known features, such as the velocity of simple vortex ring, and the stability calculation for a jet [see Batchelor and Gill, J. Fluid Mech. **14**, 529 (1962)]. We thank a referee for the former observation.
[38]W. Ashurst and D. Meiron, Phys. Rev. Lett. **58**, 1632 (1987).
[39]Y. Oshima and S. Asaka, J. Phys. Soc. Jpn. **42**, 708 (1977). See, in particular, Fig. 6.
[40]M. T. Landahl, J. Fluid Mech. **56**, 775 (1972).
[41]P. G. Drazin and W. H. Reid, *Hydrodynamic Stability* (Cambridge U.P., New York, 1981).
[42]H. Aref and E. D. Siggia, J. Fluid Mech. **100**, 705 (1980).